

**Taylor dispersion analysis in fused silica capillaries: a  
tutorial review**

Journal:	<i>Analytical Methods</i>
Manuscript ID	AY-TRV-04-2021-000588.R1
Article Type:	Tutorial Review
Date Submitted by the Author:	30-Apr-2021
Complete List of Authors:	Moser, Meagan; The University of Tennessee Knoxville Department of Chemistry, Chemistry; New Mexico State University Department of Chemistry and Biochemistry, Baker, Christopher; New Mexico State University Department of Chemistry and Biochemistry, Chemistry

Tutorial review article for submission to:

*Analytical Methods*

# **Taylor dispersion analysis in fused silica capillaries: a tutorial review**

Meagan R. Moser<sup>†,§</sup> and Christopher A. Baker<sup>\*, §</sup>

<sup>†</sup>Department of Chemistry, University of Tennessee, Knoxville, Tennessee, 37996, United States

<sup>§</sup>Department of Chemistry and Biochemistry, New Mexico State University, Las Cruces, New Mexico, 88003

\* Corresponding Author  
Christopher A. Baker

Address: MSC 3C, PO Box 30001, Las Cruces, NM 88003

E-mail: [cabaker@nmsu.edu](mailto:cabaker@nmsu.edu)

Phone: 575-646-1015

## ABSTRACT

Biological and pharmaceutical analytes like liposomes, therapeutic proteins, nanoparticles, and drug-delivery systems are utilized in applications, such as pharmaceutical formulations or biomimetic models, in which controlling their size is often critical. Many of the common techniques for sizing these analytes require method development, significant sample preparation, large sample quantities, and lengthy analysis times. In other cases, such as DLS, sizing can be biased towards the largest constituents in a mixture. Therefore, there is a need for more rapid, sensitive, accurate, and straightforward analytical methods for sizing macromolecules, especially those of biological origin which may be sample-limited. Taylor dispersion analysis (TDA) is a sizing technique that requires no calibration and consumes only nL - pL sample volumes. In TDA, average diffusion coefficients are determined via the Taylor-Aris equation by characterizing band broadening of an analyte plug under well-controlled laminar flow conditions. Diffusion coefficient can then be interpreted as hydrodynamic radius ( $R_H$ ) via the Stokes-Einstein equation. Here, we offer a tutorial review of TDA, intended to make the method better understood and more widely accessible to a community of analytical chemists and separations scientists who may benefit from the unique advantages of this versatile sizing method. We first provide a tutorial on the fundamental principles that allow TDA to achieve calibration-free sizing of analytes across a wide range of  $R_H$ , with an emphasis on the reduced sample consumption and analysis times that result from utilizing fused silica capillaries. We continue by highlighting relationships between operating parameters and critically important flow conditions. Our discussion continues by looking at methods for applying TDA to sample mixtures via algorithmic approaches and integration of capillary electrophoresis and TDA. Finally, we present a selection of reports that demonstrate TDA applied to complex challenges in bioanalysis and materials science.

## INTRODUCTION

Designing and producing drug delivery systems, therapeutic proteins, nanoparticles, and biopolymers requires fast and straightforward characterization of these products via high accuracy and high sensitivity analytical methods. Many standard methods for solution-phase size characterization require extensive method development, tedious sample preparation, large sample volumes, lengthy analysis times, and/or expensive instrumentation. One widely used size characterization method is dynamic light scattering (DLS), which can, in some cases, be performed with limited sample preparation and offer rapid analysis times. Complex samples such as blood plasma have been analyzed by DLS with preparation as simple as dilution, filtration and/or centrifugation.<sup>1, 2</sup> However, signal intensity in DLS is proportional to the analyte radius raised to the 6<sup>th</sup> power,<sup>3</sup> which makes detection sensitivity particularly challenging when characterizing small particles. For the same reason, DLS is sensitive to issues of analyte aggregation.<sup>3</sup> These qualities are often disadvantageous when interrogating the size of small proteins, especially in the presence of larger proteins or

1  
2  
3 aggregates. Hawe *et al.* measured a range of concentrations (0.05 – 50 mg mL<sup>-1</sup>) of  
4 various peptides and proteins.<sup>4</sup> While DLS accurately sized the antibody drug  
5 adalimumab (5 - 6 nm) at the lowest concentration, sizing the peptide oxytocin (~0.8  
6 nm) was not possible at low concentrations due to the influence of dust or excipients in  
7 the sample. In this case, DLS provided inaccurate and inconsistent hydrodynamic  
8 radius ( $R_H$ ) determinations for oxytocin ranging from 6.9 – 130 nm. In the same work,  
9 DLS was utilized to observe aggregation in heat-stressed formulations of protein  
10 samples. With a 5°C increase in temperature, a model IgG antibody showed an  
11 increase from  $R_H = 7.5$  nm to  $R_H = 22$  nm by DLS, whereas TDA measured a modest  
12 increase from  $R_H = 6.5$  nm to  $R_H = 7.5$  nm under identical conditions. This disagreement  
13 was attributed to the bias of DLS towards large particles, in which the largest particles  
14 or aggregates dominate the overall scattering intensity, thus resulting in inaccurately  
15 high  $R_H$  determinations.  
16  
17  
18

19 Size exclusion chromatography (SEC) is another method often employed for size  
20 determination. SEC requires precise calibration with appropriate size standards, and is  
21 susceptible to deleterious effects of analyte-column interactions.<sup>5</sup> Pacáková *et al.* found  
22 that melittin, a strongly basic peptide found in bee venom, displayed deleterious  
23 retention on a hydrophilic SEC column, which they attributed to the peptide's inability to  
24 form a predominantly hydrophilic shell due to the uneven distribution of exterior  
25 hydrophilic residues.<sup>6</sup> Overcoming these deleterious analyte-column interactions  
26 required method optimization such as the addition of an organic solvent to the mobile  
27 phase and pH optimization. Ricker *et al.* explain that SEC columns can exhibit  
28 electrostatic effects when the mobile phase ionic strength is low, and hydrophobic  
29 effects when ionic strength is high.<sup>7</sup> Either case can result in deleterious retention of  
30 analytes, which can result in peak deformation and, ultimately, inaccuracy of size  
31 determinations by SEC. They observed the effect of mobile phase ionic strength on  
32 SEC of three mouse myeloma antibodies using a silica-based stationary phase material.  
33 At low ionic strength, the least basic antibody had no net positive charge, and was  
34 therefore unaffected by adsorption to the anionic silanols at the stationary phase  
35 surface. However, at high ionic strength, the antibody was retained due to hydrophobic  
36 effects. This work demonstrates the careful consideration for method development that  
37 is needed for accurate size determinations by SEC.  
38  
39  
40  
41

42 Various micro- and nanoscopic imaging techniques such as transmission  
43 electron microscopy (TEM), scanning electron microscopy, and atomic force microscopy  
44 have been applied to particle sizing.<sup>8-14</sup> However, field of view ultimately limits the  
45 throughput of analysis for any imaging technique applied to molecular or particle sizing.  
46  
47

48 Taylor dispersion analysis (TDA) is a powerful analytical method for size  
49 characterization that addresses many of the shortcomings of the more common  
50 methods described above. Size determinations by TDA are absolute, requiring no  
51 calibration nor prior knowledge of sample concentration.<sup>15</sup> TDA conducted in fused  
52 silica capillaries requires only sub-nanoliter sample volumes, and the method can be  
53 applied to sizing analytes from small molecules<sup>16-20</sup> to micron-scale particles and  
54 complexes.<sup>21, 22</sup> TDA has evolved from studying gaseous diffusion coefficients in large  
55  
56  
57  
58  
59  
60

1  
2  
3 tubes<sup>23-25</sup> to TDA measurements of therapeutic proteins,<sup>26-36</sup> drug delivery systems,<sup>26, 30,</sup>  
4 <sup>37-42</sup> nanoparticles,<sup>43-52</sup> mixtures,<sup>15, 44, 53-59</sup> synthetic polymers,<sup>30, 60-64</sup> and more. While  
5 TDA has been discussed in other reviews of physicochemical characterization methods  
6 in specific application areas,<sup>65-70</sup> to our knowledge no recent review has combined a  
7 tutorial discussion of the underlying principles and practical considerations of TDA with  
8 an outline of the breadth and depth of modern TDA applications. Here, we offer a  
9 tutorial review of TDA, intended to make the method better understood and more widely  
10 accessible to a community of analytical chemists and separations scientists who may  
11 benefit from the unique advantages of this versatile sizing method.  
12  
13  
14  
15

## 16 PRINCIPLES OF TDA

17  
18 First described by Taylor in 1953,<sup>23</sup> TDA enables the direct determination of  
19 diffusion coefficients across a wide range of hydrodynamic radii ( $\text{\AA}$  -  $\mu\text{m}$ ). TDA is a  
20 mathematical framework for analyzing dispersion that results from the interaction  
21 between the parabolic velocity profile of pressure driven laminar flow in a cylindrical  
22 tube and the radial diffusion of analytes across that velocity profile. A sample plug  
23 injected into flow spreads axially due to the combined effects of convection and  
24 diffusion, which is observed as band broadening (Fig. 1). Diffusion occurs both radially  
25 and longitudinally, however TDA is conducted under well-controlled flow conditions  
26 (discussed in more detail below) that ensure the contribution to band broadening from  
27 longitudinal diffusion is negligible. As a result of the parabolic velocity profile, the initial  
28 velocity of any individual analyte molecule or particle is a function of its starting radial  
29 position within the injected sample plug. As radial diffusion proceeds, each molecule or  
30 particle samples the full range of flow velocities in the parabolic profile over the duration  
31 of flow, resulting in an ensemble average velocity across all particles in the sample  
32 population.  
33  
34  
35

36 Analytes with low diffusion coefficients move slowly across the parabolic velocity  
37 profile such that two analyte particles starting with disparate velocities remain separated  
38 within their respective flow streams for a longer duration as compared to the behavior of  
39 analytes with higher diffusion coefficients. The net result is a broad distribution of  
40 velocities about the population mean velocity for analytes with low diffusion coefficients,  
41 which is observed as a high degree of band broadening. Conversely, molecules with  
42 relatively high diffusion coefficients move rapidly across the parabolic velocity profile,  
43 experiencing a narrower distribution of velocities about the population mean, thus a  
44 lower degree of band broadening is observed.  
45

46 It is worth noting here that the relationship between diffusion coefficient and band  
47 broadening observed by TDA may seem counterintuitive to many separations scientists  
48 more accustomed to considering *longitudinal* diffusion. By the mechanism of  
49 longitudinal diffusion, higher rates of diffusion result in increased band broadening,  
50 which is the opposite of what is described above. Nevertheless, when considering *only*  
51 *radial diffusion* in TDA measurements, molecular diffusion coefficients ( $D$ ) can be  
52 determined by observing the degree of band broadening as follows:<sup>71, 72</sup>  
53  
54  
55  
56  
57  
58  
59  
60

$$D = \frac{R_c^2 t_d}{24\sigma^2} \quad (1)$$

where  $R_c$  is the channel radius,  $t_d$  is the average elution time, and  $\sigma^2$  is the peak variance.  $D$  can be used as a structural descriptor of the analyte when transformed to  $R_H$  via the Stokes-Einstein relation:<sup>73</sup>

$$R_H = \frac{k_B T}{6\pi\eta D} \quad (2)$$

where  $k_B$  is the Boltzmann constant,  $T$  is temperature, and  $\eta$  is the dynamic viscosity of the solution.

For TDA to yield accurate determinations of  $D$ , precise control of flow is required to meet two requisite conditions known as the Taylor conditions. First, TDA considers radial diffusion while neglecting longitudinal diffusion. For this to be possible, the rate of advection must be significantly greater than the rate of diffusion, which is widely considered to be satisfied when the Péclet number ( $Pe$ ) is greater than 69.<sup>74</sup>  $Pe$  is defined for a cylindrical channel as:<sup>72</sup>

$$Pe = \frac{uR_c}{D} \quad (3)$$

where  $u$  is the linear flow rate. In his original work,<sup>74</sup> Taylor defined the following inequality as a requirement to satisfy eqn (1):

$$\frac{4L}{R_c} \gg \frac{uR_c}{D} \gg 6.9 \quad (4)$$

where  $L$  is the length of the channel. In that work, a ratio of 1:10 between the inequalities was considered requisite, which gives the accepted Taylor condition  $Pe \geq 69$ . Cottet *et al.* demonstrated that longitudinal diffusion can be neglected even in conditions where  $Pe < 69$ , defining requisite flow velocity as:<sup>56</sup>

$$u \geq \frac{D}{R_c} \sqrt{\frac{48}{\varepsilon}} \quad (5)$$

where  $\varepsilon$  is the relative error in determination of  $D$ . By this analysis, Taylor's condition of  $Pe \geq 69$  gives a relative error due to neglecting longitudinal diffusion of 1%, whereas Cottet and coworkers suggest that a relative error of 3% can be tolerated, leading to the requisite condition  $Pe \geq 40$ .

The second Taylor condition describes the duration for which a sample plug must remain in flow in order to observe sufficient band-broadening effects due to Taylor dispersion. Taylor's original work described the condition as follows: "the time necessary for appreciable effects to appear, owing to convective transport [must be]

long compared with the ‘time of decay’ during which radial variations of concentration are reduced to a fraction of their initial value through the action of molecular diffusion”.<sup>23</sup> As such, the requisite residence time ( $t_R$ ) of the sample plug in flow is influenced by  $D$  and  $R_c$ . Residence time can be normalized for these factors to give a dimensionless time factor ( $\tau$ ) defined as:

$$\tau = \frac{Dt_R}{R_c^2} \quad (6)$$

Taylor expresses Inequality (4) as the inequality<sup>74</sup>

$$D \gg \frac{R_c^2}{4t_R} \quad (7)$$

Taking a 1:10 ratio as satisfying Inequality (7), the following condition satisfies minimum required  $t_R$ :

$$t_R \geq 2.5 \frac{R_c^2}{D} \quad (8)$$

Substituting  $t_R$  in eqn (6) with Inequality (8), we can obtain the minimum required value for  $\tau$ :

$$\tau = \frac{Dt_R}{R_c^2} = \frac{D \left( 2.5 \frac{R_c^2}{D} \right)}{R_c^2} \geq 2.5 \quad (9)$$

Alternative minimum  $\tau$  values have also been reported. In the same work that studied alternative minimum  $Pe$  conditions, Cottet *et al.* demonstrate that the minimum  $t_R$  can also be expressed as a function of  $\varepsilon$  as follows<sup>56</sup>

$$t_R \geq \frac{3R_c^2}{80D\varepsilon} \quad (10)$$

Presuming an acceptable  $\varepsilon$  of 3%, Inequality 10 becomes:

$$t_R \geq \frac{1.25R_c^2}{D} \quad (11)$$

Substituting  $t_R$  in eqn (6) with Inequality (11), we can obtain the minimum required value for  $\tau$ :

$$\tau = \frac{Dt_R}{R_c^2} = \frac{D \left( 1.25 \frac{R_c^2}{D} \right)}{R_c^2} \geq 1.25 \quad (12)$$

1  
2  
3  
4 There is some disagreement on appropriate limiting value of  $\tau$ . Several works report the  
5 condition  $\tau > 1.4$ .<sup>45, 72, 75, 76</sup> However, to our knowledge, no mathematical basis for  
6 alternate limiting  $\tau$  values has been offered with the rigor of either Taylor or Cottet's  
7 solutions shown above.  
8  
9

## 10 PRACTICAL CONSIDERATIONS FOR TDA MEASUREMENTS

11  
12 Several practical considerations arise from the requisite Taylor conditions. First,  
13 eqn (4) shows that analysis times can be dramatically reduced by reducing  $R_c$ . This has  
14 motivated the use of fused silica capillaries (typ. 10 - 250  $\mu\text{m}$  i.d.) as flow systems for  
15 TDA. As a result, capillary electrophoresis (CE) instrumentation has become a  
16 prominent tool in the continued development and application of TDA. Second, although  
17 TDA is a method for determining  $D$ , target values of  $D$  are needed to define the requisite  
18 Taylor conditions. Since the Taylor conditions are met by exceeding thresholds (i.e.  $\tau \geq$   
19  $2.5$  and  $Pe \geq 69$ ), *a priori* knowledge of  $D$  is not required. Instead, careful consideration  
20 is needed to bracket an appropriate range of  $D$  values for a given analysis, which can  
21 be used to deduce the limiting values of operating parameters  $u$ ,  $R_c$ , and  $t_R$  that satisfy  
22 the Taylor conditions. Finally, it is impractical to consider the two requisite Taylor  
23 conditions independently when designing the parameters of a TDA experiment. For  
24 example,  $Pe$  must exceed a value of 69 but is given no theoretical upper bound, which  
25 suggests there is no upper bound of the operating parameter  $u$  and therefore flow  
26 velocity should be maximized. While  $u$  is not given an upper bound on the basis of  
27 theory, increasing  $u$  requires increasing capillary length in order to achieve a value for  $t_R$   
28 to satisfy  $\tau > 2.5$ , and impractical capillary lengths can quickly arise from poorly chosen  
29  $u$  values. Thus, practical limitations require a careful selection of operating parameters  
30 to meet the Taylor conditions for an appropriately bracketed range of  $D$ . With careful  
31 consideration, and several iterative calculations of eqn (3) and Inequality (4), selecting  
32 appropriate and practical operating conditions for TDA is not prohibitively laborious. Still,  
33 making available purpose-built calculation tools for establishing appropriate operating  
34 parameters would benefit researchers currently utilizing TDA and may foster more  
35 widespread adoption of the technique.  
36  
37  
38  
39  
40

41  
42 Practical and theoretical limitations exist beyond the scope of appropriately  
43 selecting operating parameters to meet the requisite Taylor conditions. For example, the  
44 TDA principles described above assume that the sample plug remains under continuous  
45 flow for the full duration of  $t_R$ . In practice, this can be difficult or impossible to achieve,  
46 especially when utilizing CE instrumentation. The act of injecting a sample plug via  
47 conventional CE injection methods necessarily gives discontinuous flow velocities  
48 because flow must be stopped to bring a sample vial to the capillary inlet and stopped  
49 again to return a buffer vial to the capillary inlet before flow recommences for the TDA  
50 procedure. A key to overcoming this limitation has been the use of dual-detector  
51 schemes,<sup>16, 17, 77, 78</sup> in which band broadening is compared between two detection points  
52 positioned on the flow path to achieve the appropriate  $t_R$  value within the volume  
53 between the detection points. In this way, band broadening evolves while under  
54 continuous flow between the two detection points, and any contribution to overall band  
55  
56  
57  
58  
59  
60



1  
2  
3 broadening from discontinuous flow in the sample injection process is accounted for in  
4 the initial observation at the first detection point. Dual-detector TDA utilizes a modified  
5 form of the Taylor-Aris equation as follows:<sup>76</sup>  
6  
7

$$D = \frac{R_c^2(t_2 - t_1)}{24(\sigma_2^2 - \sigma_1^2)} \quad (13)$$

8  
9  
10  
11  
12 where  $t_1$  and  $t_2$  are the peak arrival times at detectors 1 and 2, respectively, and  $\sigma_1^2$  and  
13  $\sigma_2^2$  are the peak variances as observed at detectors 1 and 2, respectively.  
14

15  
16 Chamieh *et al.* compared the performance of TDA in single- and dual-point  
17 detection configurations.<sup>53</sup> In their work, TDA of monodisperse albumin proteins and  
18 polydisperse polymer standard samples was performed utilizing a commercial CE  
19 instrument equipped with a 60 cm x 50  $\mu\text{m}$  i.d. fused silica capillary and UV absorbance  
20 detector. For single-point detection, band broadening was analyzed for signals collected  
21 at three detector positions (effective capillary lengths: 8.5 cm, 24.5 cm, and 51.5 cm).  
22 For dual-point detection, signals were analyzed with detection points positioned at 24.5  
23 cm and 51.5 cm. Unsurprisingly, single-point detection TDA resulted in overestimates of  
24  $R_H$  when the injection volume was a significant fraction ( $> 1\%$ ) of the total effective  
25 capillary volume. Utilizing previously reported mathematical corrections<sup>17</sup> for the effects  
26 of pressure ramping and the finite volume of the injection plug,  $R_H$  determinations by  
27 single-point detection TDA were not statistically different from those determined by dual-  
28 point detection, provided injection volume remained  $< 1\%$  of effective capillary volume.  
29 However, dual-point detection TDA is arguably preferable, as it does not require any  
30 mathematical corrections or presumptions of dynamic flow conditions which may be  
31 difficult to observe. To facilitate precision TDA, technologies have been developed to  
32 achieve dual-detector configurations in commercial CE instrumentation for UV  
33 absorbance<sup>17</sup> and fluorescence detection<sup>16</sup> modes.  
34  
35

36  
37 TDA analysis times are significantly reduced by decreasing  $R_c$ , which has  
38 motivated the use of fused silica capillaries. Precise control of applied pressures to a  
39 capillary flow system can be achieved with modern commercial CE instrumentation,  
40 making these instruments well suited for TDA. Williams and Vigh leveraged the  
41 integration of CE and TDA in a commercial instrument by first separating analytes by  
42 CE then switching to pressure driven flow to perform TDA on the separated analytes.<sup>79</sup>  
43 One critical challenge to performing TDA in a commercial CE instrument was described  
44 by Sharma *et al.*, who described the effects of the initial ramp in flow velocity that occurs  
45 upon pressure application.<sup>72</sup> This non-uniform velocity profile introduces significant error  
46 in determinations of  $D$ . To circumvent this effect, ramp rate can be characterized and  
47 corrected for mathematically. The ramp rate of the CE instrument must be determined  
48 and used to convert the observed residence time to the ideal residence time by the  
49 equation:  
50  
51

$$t_R = \frac{t_{R,obs} + \sqrt{t_{R,obs}^2 - 16L_T L_D \eta / R_c^2 r_i}}{2} \quad (14)$$

where  $L_T$  is capillary length,  $L_D$  is tube length from inlet to detector, and  $r_i$  is the rate of increase of applied pressure. When there is no initial velocity ramp,  $t_R = t_{R,obs}$  and  $D$  can be determined simply by eqn (1). However, a velocity ramp leads to errors in the measured values of  $D$  if not corrected using eqn (14). With increased  $t_{R,obs}$  the effect of  $r_i$  becomes negligible, and as  $t_{R,obs}$  approaches infinity, any error in  $D$  would approach zero. Thus, the effect of the ramp is greater at lower  $t_{R,obs}$ . To demonstrate this, the error in  $D$  determinations for phenylalanine was characterized as a function of  $t_{R,obs}$ . Errors greater than 50% were observed for  $t_{R,obs} < 50$  s whereas  $<1\%$  error was observed for  $t_{R,obs} > 100$  s. Correcting for flow velocity ramp by eqn (14), reduced the error at all  $t_{R,obs}$  evaluated to  $<2\%$ . While this correction was straightforward for frontal analysis, zonal analysis required additional corrections to account for the finite width of the injection plug. The additional correction required the calibration of observed peak variance ( $\sigma_{obs}^2$ ) vs injection volume ( $V_i$ ) at each  $t_R$ . Thus, correcting for a velocity ramp in zonal analysis can add substantial additional work to the overall workflow.

The operating principles of TDA are conceptually similar to those of hydrodynamic chromatography (HDC), although these are mechanistically distinct modes of analysis. Cottet and coworkers characterized the relationship between  $R_H$ , applied pressure, and capillary diameter to elucidate the conditions under which HDC mechanisms interfere with the accurate interpretation of TDA results.<sup>80</sup> In Figs. 2A and 2B, the red lines correspond to experimental conditions of constant analyte size (vertical line) or constant mobilizing pressure (horizontal lines), and the dots represent the conditions illustrated in Figs. 2C and 2D. When 250 nm polystyrene nanoparticles (PS NPs) were analyzed by TDA utilizing a 50  $\mu\text{m}$  i.d. fused silica capillary under mobilization pressures from 7 – 550 mbar, peak shape became distorted at and above 90 mbar (Fig. 2C). Interestingly, the conditions with observed peak distortion corresponded to  $\tau \leq 1.25$ , which fails to satisfy the requisite Taylor condition. When various sizes of PS NPs ( $R_H = 110$  nm, 250 nm, 500 nm) were analyzed by TDA utilizing 25  $\mu\text{m}$  i.d. fused silica capillary and a fixed mobilizing pressure of 28 mbar, the effects of HDC reduced elution times of 250 nm and 500 nm PS NPs (Fig. 2D). Importantly, HDC affected the variance of the NP peaks even without appreciable effects on mean elution time, which adversely affected the accuracy in determinations of  $D$ . The authors identified an upper limit on the ratio of  $R_H$  to capillary radius ( $R_C$ ) as a function of  $\varepsilon$  given by:

$$\frac{R_H}{R_C} = 0.17\varepsilon \quad (15)$$

In many cases, especially when designing TDA experiments for the analysis of macromolecular constructs, this constraint will warrant careful consideration when selecting appropriate operating parameters to meet the Taylor conditions.

Another important consideration is the potential for analyte-capillary adsorption, which will introduce peak asymmetry in the resulting elution profile, or taylorgram. Latunde-Dada *et al.* observed asymmetric peaks with pronounced tailing in varying concentrations of lysozyme (1 - 20 mg mL<sup>-1</sup>) in a standard 75  $\mu\text{m}$  i.d. capillary.<sup>81</sup> As an attempt to mitigate the effect of peak tailing on  $R_H$  determinations, they developed a

1  
2  
3 constrained fitting algorithm to isolate dispersive components of the concentration  
4 profiles from the solute-capillary interacting components. This mathematical correction  
5 yielded improved accuracy in  $R_H$  determinations for high concentration (i.e. 5 - 20 mg  
6 mL<sup>-1</sup>) lysozyme samples. Interestingly, at 1 mg mL<sup>-1</sup> lysozyme, both free and  
7 constrained fits gave inaccurate  $R_H$  determinations ( $4.5 \pm 0.3$  nm and  $3.33 \pm 0.03$  nm,  
8 for free and constrained fits, respectively as compared to previously reported values of  
9 1.89 - 2.05 nm<sup>82, 83</sup>). The authors postulated that these inaccuracies resulted from a  
10 much greater fraction of total sample engaged in adsorptive interactions at the capillary  
11 wall and, thus, subject to a net flow velocity that did not meet the Taylor criteria. Here,  
12 we suggest that adverse adsorption effects may warrant adapting common practices  
13 from CE methods, such as capillary surface modification or buffer additives,<sup>61, 84, 85</sup> for  
14 use in TDA measurements. Such efforts will require careful consideration and  
15 characterization of the effects on solution viscosity to yield accurate calibration-free size  
16 determinations.  
17  
18  
19

20  
21 Though the principles of TDA were first described in the early 1950s, modern  
22 capillary flow systems have enabled this technology to be leveraged more recently as a  
23 powerful technique for size determination in various application areas and across  
24 various modes of analysis. For example, in addition to UV absorbance<sup>17</sup> and  
25 fluorescence detection<sup>16, 86</sup> modes, TDA has been coupled to mass spectrometry,<sup>87, 88</sup>  
26 refractive index detection,<sup>62</sup> and backscattering interferometry.<sup>89</sup> To this point, we have  
27 considered TDA of pure substances. TDA leverages tools common to separation  
28 science, and therefore it is interesting to examine how the practice and principles of  
29 TDA become more complex in the context of sample mixtures.  
30  
31

## 32 **ALGORITHMIC APPROACHES TO TDA OF MIXTURES**

33

34 TDA is applicable to both monodisperse and polydisperse samples.<sup>53, 55</sup> For  
35 monodisperse samples, TDA results for the determination of  $R_H$  are directly analogous  
36 to those of DLS, which is a standard method for particle size characterization.<sup>55</sup>  
37 Conventionally, TDA gives weight-averaged or number averaged  $R_H$  values when  
38 utilizing mass- or concentration-sensitive detection modes, respectively.<sup>15</sup> Thus, the  
39 resulting  $R_H$  determinations for polydisperse samples can differ from the harmonic z-  
40 averaged  $R_H$  value obtained by DLS.<sup>90</sup> This incongruency with DLS has motivated  
41 various regression and statistical analysis approaches to improve the performance of  
42 TDA for mixtures and polydisperse samples.  
43  
44  
45

46 Common peak fitting methods for non-Gaussian peak shapes have been applied  
47 to TDA data for the analysis of polydisperse samples. Deviations from a strict Gaussian  
48 peak shape were observed at the apex and base of taylorgrams produced from a  
49 mixture of third and fifth generation dendrigraft poly-L-lysine, complicating the  
50 determination of appropriate peak variance in the taylorgram.<sup>53</sup> In the case where  
51 Gaussian fits cannot be applied to taylorgrams of polydisperse samples, peak variance  
52 can be determined via an integration-based algorithm. In that work, peak variance was  
53 determined by integrating the whole signal of the resulting non-gaussian peaks across  
54 the time interval using the following equation:  
55  
56  
57  
58  
59  
60

$$\sigma^2 = \frac{\int h(t)(t - t_d)^2 dt}{\int h(t) dt} = \frac{\sum_m^{i=n} h_i(t_i - t_d)^2(t_{i+1} - t_i)}{\sum_m^{i=n} h_i(t_{i+1} - t_i)} \quad (16)$$

where  $h(t)$  is detector response,  $t_i$  is elution time for a given point  $i$ ,  $t_d$  is the average elution time,  $n$  and  $m$  are the starting and ending points considered for the integration. This integration method yielded a weight-average  $R_H$  determination. Furthermore, this method depended heavily on the selection of the boundaries for integration, defined by the variables  $n$  and  $m$ . Several boundaries were considered defined by cutoff lines ranging from 0 - 2% of the peak apex (Fig. 3A). Fig. 3B compares the results of the integration method (data points) with the results of conventional gaussian fitting (horizontal dashed lines). A general trend of reduced mean  $R_H$  with increased cutoff percentage was observed. Comparison of the mean  $R_H$  values obtained from the integral and gaussian fitting methods revealed no significant difference and agreement with 95% confidence. However, for third and fifth generation dendrigraft poly-L-lysine (G3 and G5), poor agreement was observed between the Gaussian fitting and integration methods at all cutoff percentages. The authors attributed this to Gaussian fitting being poorly suited for the irregular peak shapes of G3 and G5. To prevent contributions from noise influencing the integration method, the cutoff line corresponding to  $4 \times \sigma_{noise}$  was defined as the appropriate threshold, which in this work corresponded to 0.75% of the peak apex (Fig. 3B, vertical dashed line).

Data analysis methods have been developed to extract multiple constituent  $R_H$  values from the taylorgrams of mixtures.<sup>15, 55, 56</sup> In one example, three independent data analysis methods were applied to monitoring a polymerization reaction by TDA.<sup>55</sup> In the first method, the degree of conversion was determined by comparing integrated areas in the taylorgrams before and after the polymerization reaction. In the second method, the taylorgrams for each component in the reaction mixtures were recorded and fitted as Gaussian curves, and the taylorgram for the reaction mixture was deconvolved by fitting as the sum of Gaussian curves for the mixture components. The third method subtracted the Gaussian contribution of the monomer mixture from the taylorgram of the reaction mixture and fitted the reduced signal iteratively to extract the polymer contribution. Three standards of polyacrylamide (PAM) with varying weight average molar masses and acrylamide (AM) monomer were analyzed by TDA individually and as AM/PAM (10:90 v:v) mixtures for each molar mass standard to mimic a polymerization medium. Peak profiles in AM/PAM mixtures were shown to be the sum of the contributions from each component, as illustrated in Fig. 4A. All three data analysis methods determined  $R_H = 0.22$  nm for AM, while  $R_H$  values for AM/PAM agreed across all methods to within 0.5 nm. TDA was performed on aliquots of an acrylamide polymerization reaction mixture at several time points, as illustrated in Fig. 4B. The three methods were separately utilized to determine  $R_H$  for the resulting PAM, and all methods agreed to within 4%.

Cipelletti described a cumulant analysis method for determining the polydispersity of moderately complex sample mixtures.<sup>54</sup> By the cumulant method, the

1  
2  
3 logarithm of any taylorgram can be expanded into a cumulant series, in which the first  
4 cumulant ( $\Gamma_1$ ) is directly related to the mean of the gamma distribution of  $D$ . The authors  
5 showed that polydispersity could be characterized by evaluating the deviation from  
6 linearity in the plot of the cumulant series. In further work, Cipelletti *et al.* described the  
7 constrained regularized linear inversion (CRLI) approach for determining probability  
8 density functions (PDFs) of  $D$  from taylorgrams.<sup>44</sup> This added additional constraints to  
9 the standard least-squares fit to overcome the difficulties of an infinite set of PDF  
10 solutions that fit the taylorgram function.  $D$  averages were determined by CRLI  
11 approach that agreed to within 10% of the expected values utilizing both simulated and  
12 experimental data, and up to 10% error was observed for determinations of  
13 polydispersity indices of various polystyrenesulfonate samples and mixtures.  
14  
15

16  
17 Latunde-Dada *et al.* described an algorithmic approach to deconvolution of  
18 taylorgrams of mixtures based on initial parameter estimations as seed values for fitting  
19 by least squares regression.<sup>57</sup> In that approach, a system of equations describing the  
20 relative contributions of various peak amplitudes and variances can be solved using  
21 initial parameters derived from the second derivative, integral, and double integral of the  
22 net taylorgram signal. The authors demonstrated the utility of their approach in various  
23 use cases, including 2, 3, and 4 component mixtures of related and unrelated analytes,  
24 and with various conditions of a priori knowledge of analyte radius. In each case,  
25 hydrodynamic radii in good agreement with nominal reported values were determined  
26 for all mixture components.  
27  
28

29  
30 These examples illustrate that fitting and deconvolution algorithms can be  
31 applied to interpreting taylorgrams of sample mixtures. Although no theoretical upper  
32 limit has been proposed for the number of mixture components that can be handled by  
33 these methods, the mathematical complexity and uncertainty inherent to such  
34 approaches suggests that they are best reserved for relatively simple mixtures.  
35 Applications requiring increased resolution and peak capacity will benefit from the  
36 common instrumentation shared by both CE and TDA, which facilitates their online  
37 integration.  
38  
39

## 40 **INTEGRATING CE AND TDA**

41  
42 As we previously discussed, dual-point detection is an effective approach to  
43 circumventing challenges of non-uniform or discontinuous flow velocities in TDA, but it  
44 presents an engineering challenge of integrating two detection points within the confines  
45 of commercial CE instrumentation. Chamieh *et al.* implemented a dual-point UV  
46 detection approach by looping the capillary inside of a standard CE capillary cassette  
47 such that it passed the UV detection point twice before exiting the cassette (Fig. 5A).<sup>17</sup>  
48 This required modification of the instrument's detection interface to allow both detection  
49 windows on the looped capillary to overlap within the same interface. Fig. 5B (top)  
50 compares the taylorgrams obtained for 75  $\mu\text{M}$  HSA using the unmodified interface (gray  
51 trace) and the modified interface (black trace). A 10-fold decrease in sensitivity was  
52 observed when using the modified detection interface, which the authors attributed to  
53 the removal of a spatial filtering slit which typically prevents transmission through the  
54  
55  
56  
57  
58  
59  
60

1  
2  
3 capillary in regions outside of the capillary inner diameter. However, reduced sensitivity  
4 did not adversely affect the observed peak variance or elution profiles of sufficiently  
5 concentrated samples, as observed by the normalized data in Fig. 5B (bottom). Dual-  
6 point UV detection was utilized to determine  $R_H$  at two mobilizing pressures (30 and 50  
7 mbar, respectively) for 10 mM caffeine ( $R_H = 0.462 \pm 0.013$  nm and  $0.436 \pm 0.017$  nm),  
8 75  $\mu$ M BSA ( $R_H = 4.10 \pm 0.12$  nm and  $4.13 \pm 0.13$  nm), and 75  $\mu$ M HSA ( $R_H = 4.19 \pm$   
9  $0.09$  nm and  $4.25 \pm 0.14$  nm) and in all cases were found to agree with literature values  
10 to within 5%.  
11  
12

13  
14 Fluorescence is often utilized as a detection mode in CE because it overcomes  
15 pathlength limitations of UV-absorbance detection in small diameter capillaries, but the  
16 integration of dual-point fluorescence detection in commercial CE instrumentation is  
17 challenging. Our group developed a miniature LED-induced fluorescence detection  
18 system for CE that was sufficiently compact to enable the integration of two detectors  
19 within the cassette of a commercial CE instrument.<sup>16</sup> The 3D printed design, shown in  
20 Fig. 5C incorporated an LED excitation source, bandpass excitation filter, pinhole  
21 collimator, and emission-collecting ball lens. Operating conditions such as LED current,  
22 and PMT gain control voltage were optimized via multivariate analysis to yield a  
23 detection limit of  $613 \pm 13$  pM for fluorescein. The system was used to monitor the  
24 progress of a fluorescent bioconjugation reaction between fluorescein isothiocyanate  
25 (FITC) and BSA, and the integration of CE-TDA with fluorescence detection was shown  
26 to enable standard-free identification of peaks in the CE separation. Fig. 5D shows the  
27 overlay of signals obtained from both detectors (solid and dashed black traces) and the  
28 corresponding Gaussian fits (solid and dashed red traces) at reaction time = 2 min. TDA  
29 of the CE-separated zones provided  $R_H$  values of 4.4 nm and 0.54 nm for peak 1 and  
30 peak 2, respectively, allowing the assignment of these peaks to FITC-BSA and free  
31 FITC, respectively.  
32  
33  
34

35  
36 CE and TDA have been used together to monitor reaction progress in other  
37 systems. Affinity CE is widely utilized for studying biomolecular interactions, and in this  
38 regard CE-TDA can offer advantages for elucidating biophysical and functional  
39 properties of binding systems. Ostergaard and Jensen demonstrated the first  
40 application of CE-TDA for the simultaneous characterization of protein-ligand binding  
41 and protein  $R_H$  in two separate affinity systems.<sup>76</sup> Advancing fronts were used to obtain  
42  $D$  and  $R_H$  values for free ligands,  $\alpha_1$ -acid glycoprotein (AGP) and human serum albumin  
43 (HSA), and for propranolol-ligand complexes to investigate and quantify their  
44 interactions. Differences in the degree of binding between propranolol-AGP and  
45 propranolol-HSA were significantly different, showing a trend in agreement with  
46 previous literature. Further, Liu *et al.* monitored surface functionalization of dendrigraft  
47 poly-L-lysines (DGL).<sup>91</sup> TDA was used to determine the  $R_H$  of the polypeptides and of a  
48 click reaction product. While the results confirmed the reaction, TDA gives a weight  
49 average  $R_H$  which does not provide information on reagent or product purity nor  
50 homogeneity. CE was used separately from, and complimentary to, TDA to characterize  
51 the reaction mixture components. Comparison of electropherograms of the clicked  
52 product spiked with the starting materials and intermediate compounds clearly  
53 illustrated the absence of these reaction components in the final product. Similarly,  
54  
55  
56  
57  
58  
59  
60

1  
2  
3 Deschamps *et al.* characterized the size of an ionic polydiacetylene by TDA while  
4 monitoring its polymerization process by CE.<sup>92</sup>  $R_H$  values for the polymer were reported  
5 as 1.77 nm and 1.9 nm by TDA and DLS, respectively, where the small difference was  
6 attributed to sample polydispersity. CE results were used in this study to determine  
7 degree of polymerization, polydispersity index, and number average molar mass. CE is  
8 also well-suited for online integration with TDA, which combines in a single analysis the  
9 high resolving power of CE with  $R_H$  determinations by TDA.<sup>93</sup> A mixture can be  
10 electrophoretically separated with high resolution while experimental traces from the  
11 same detector are recorded and used for TDA. Several groups have reported success  
12 in on-line integration of CE-TDA for monitoring of bioconjugation reactions,<sup>16, 76</sup>  
13 nanoparticle characterization,<sup>49, 50, 78, 94</sup> characterization of charged complexes,<sup>93, 95</sup> and  
14 more.

15  
16  
17 Characterizing the 3D structure of proteins and biomolecules is critical in  
18 understanding their biological function. Xu and coworkers developed mobility capillary  
19 electrophoresis (MCE) to circumvent challenges associated with common structural  
20 analysis techniques.<sup>96, 97</sup> MCE combines CE with suppressed electroosmotic flow and  
21 TDA to enable determinations of  $R_H$  and effective ionic charge from a single experiment.  
22 MCE has been demonstrated in combination with mass spectrometry and molecular  
23 dynamics simulations for 3D protein structural analysis from solution-phase samples.  
24 MCE has been applied to a variety of proteins and protein mixtures, under native  
25 conditions and non-native pH conditions.<sup>98, 99</sup>

26  
27 The characterization of size and function in non-biological systems by CE-TDA  
28 has also been reported. Leclercq and Cottet proposed a methodology for the  
29 characterization of polyelectrolyte complexes in which a CE separation of constituents  
30 followed by TDA allows for the determination of charge stoichiometry and  $R_H$ ,  
31 respectively.<sup>95</sup> Oukacine *et al.* utilized the high separation performance of CE in  
32 conjunction with the absolute size determination of TDA for the determination of  $R_H$  of a  
33 bimodal mixture of nanolatexes (56 and 70 nm in size).<sup>78</sup> First, a baseline separation of  
34 the two nanolatexes by CE was required before TDA could be performed. A UV detector  
35 and capillary with three detection windows in a looped configuration was used in this  
36 study. Reported values of  $D$  were in good agreement with values obtained by TDA of  
37 the two nanolatexes individually, ultimately demonstrating CE-TDA as a suitable  
38 approach for the characterization of mixtures of nanoparticles similar in size.

## 41 42 **APPLICATIONS OF TDA TO BIOANALYSIS**

43  
44  
45 Analysis of biological and pharmaceutical compounds can take advantage of the  
46 low sample volumes of TDA, since sample availability in these cases can be limiting.<sup>54</sup>  
47 Such compounds include therapeutic peptides and proteins,<sup>26-29, 31-35</sup> drug delivery  
48 systems,<sup>30, 37, 38</sup> and lipids.<sup>39-42</sup> Diffusion and transport through tissue mimics, hydrogels,  
49 and capillaries has also been modeled for biological applications.<sup>30, 31, 100</sup>

50  
51 Hulse *et al.* demonstrated TDA for the size characterization of therapeutic  
52 proteins and their respective aggregates.<sup>28</sup> 60 nL of 10 mg mL<sup>-1</sup> bovine serum albumin  
53 (BSA) were prepared and analyzed in less than 3 minutes using a commercial TDA  
54 instrument.  $R_H$  was determined to be 4.18 nm with an RSD of 0.24%, which was in  
55 agreement with previously reported values of 3.3 - 4.3 nm. Aggregation was induced in  
56  
57  
58  
59  
60

1  
2  
3 two samples of BSA via heat stress. Comparing average  $R_H$  values of BSA determined  
4 by DLS and TDA, it was determined that greater repeatability was achieved with TDA,  
5 indicated by <1% RSD as compared to 7.09% RSD by DLS in each aggregated sample.  
6

7 Høgstedt *et al.* assessed protein-protein and peptide-peptide interactions (PPIs)  
8 by TDA.<sup>27</sup> PPIs can be characterized by the diffusion interaction parameter,  $k_D$ , which is  
9 observed as the slope of the linear fit in a plot of  $D$  vs analyte concentration. A  
10 comparison of TDA and DLS for characterizing PPIs in model peptides was not possible  
11 since, the authors reported, DLS lacked appropriate detection sensitivity for the model  
12 peptides. Therefore, TDA and DLS were compared for characterizing PPIs for the  
13 proteins  $\alpha$ -lactalbumin and HSA with highly comparable results. The higher sensitivity of  
14 TDA enabled observation of repulsive and attractive PPIs in a set of three model  
15 peptides. Furthermore, Latunde-Dada *et al.* proposed a method for obtaining  
16 concentration dependent diffusion coefficients and  $k_D$  in a single measurement by  
17 measuring dispersion as a function of concentration along the front of a sample slug.<sup>18</sup>  
18 For the application to caffeine and BSA solutions, the values and signs of  $k_D$  as well as  
19 the values of  $D$  were in good agreement with literature values and DLS results.  
20  
21

22 Protein-ligand interactions have also been studied by TDA coupled to mass  
23 spectrometry (TDA-MS). Hong *et al.* investigated noncovalent interactions of lysozyme  
24 and cytochrome C with tri-N-acetylchitotriose.<sup>87</sup> A home-built sample introduction  
25 system utilizing branched capillary channels and constant pressure pumping enabled  
26 two-point detection TDA-MS via electrospray ionization. Peaks corresponding to the  
27 protein, ligand, and the protein-ligand complex were well resolved by MS, and effective  
28 charges were determined. Ion chromatograms from the mass spectra were used for  $R_H$   
29 determinations by TDA. TDA results showed a 6.963% and 7.53% increase in  $R_H$  of  
30 lysozyme and cytochrome C, respectively, after incubation with the ligand, indicative of  
31 protein-ligand binding.  
32

33 Nanoscale hydrogels are utilized as drug delivery systems, enabling spatial,  
34 temporal, and stimulus-controlled drug release. Size characterization of these nanogel  
35 delivery systems is important, since size distribution influences *in vivo* diffusion,  
36 biodistribution, and ultimately the biological fate of these drug delivery vehicles.<sup>30</sup>  
37 Several studies have been successful in characterizing these drug delivery systems via  
38 TDA. Ibrahim *et al.* have worked to characterize the size and effective charge of a  
39 polymeric nanogel by TDA and CE, respectively.<sup>30</sup> Four copolymer nanogels were sized  
40 by TDA, resulting in an RSD of <2.2% for all  $R_H$  values, while effective ionic charge ( $Z_{\text{eff}}$ )  
41 was determined for each nanogel from electrophoretic mobility and  $R_H$ . Jensen *et al.*  
42 have also studied hydrogel matrices as drug delivery systems, but as a subcutaneous  
43 tissue mimic.<sup>31</sup> A UV imaging method was combined with TDA to visualize and  
44 characterize diffusivity and self-association behavior of insulin within an agarose  
45 hydrogel matrix in real-time. At various concentrations, insulin monomers and hexamers  
46 were easily distinguished by TDA. Low concentrations (0.1 and 0.2 mM) and pH (3.0)  
47 resulted in  $R_H = 1.5 \pm 0.1$  nm, representing the monomeric form of insulin, and high  
48 concentrations (1 mM) and moderate pH (7.4) resulted in  $R_H = 3.0 \pm 0.1$  nm, indicative  
49 of the insulin hexamer. The authors reported that DLS was less sensitive to these small  
50 changes in hydrodynamic radius.  
51  
52

53  
54 Ye *et al.* demonstrated the application of TDA to characterizing  $D$  and  $R_H$  values  
55 of drug substances in water and various pharmaceutical media (acetonitrile, methanol,  
56  
57  
58  
59  
60



isopropyl myristate, medium chain triglyceride, and propylene glycol), along with simultaneous measurements of solvent viscosity.<sup>37</sup> Relative solvent viscosity measurements were made using the two detection windows and water as a reference viscosity standard by the following equation:

$$\eta = \frac{\eta_{water}(t_{2,s} - t_{1,s})}{t_{2,water} - t_{1,water}} \quad (17)$$

where  $\eta$  is the relative solvent viscosity,  $\eta_{water}$  is water viscosity,  $t_{1,s}$  and  $t_{2,s}$  are the times at which the analyte in the solvent reaches detection windows 1 and 2, respectively, and  $t_{1,water}$  and  $t_{2,water}$  are the times at which the analyte in water reaches detection windows 1 and 2, respectively. Viscosity was determined for all solvents with RSD <1%. This work highlights the importance of considering solvent viscosity in  $R_H$  determinations, since  $D$  significantly decreases with increasing solvent viscosity, which can lead to overestimation of  $R_H$ . Simultaneous determination of solvent viscosity and  $D$  by TDA offers a promising approach to circumventing this problem.

Surfactant micelles or microemulsions are used as drug delivery systems to improve the solubility and bioavailability of drugs with poor water solubility. Formulations of these lipid-based excipients can be complex and, as with other drug delivery systems, their size characteristics will impact the efficacy of the drug delivery system. Chamieh *et al.* have made significant contributions to the characterization of micelles and microemulsions by TDA. TDA is well suited to this purpose because it is less sensitive than DLS to deleterious effects from aggregates, and variation in viscosity of micellar solutions can readily be accounted for. The effect of concentration and temperature on the size of commercial self-emulsifying pharmaceutical excipients was investigated by TDA and results compared to DLS measurements. The two excipients studied, Labrasol<sup>®</sup><sup>40</sup> and Gelucire<sup>®</sup> 44/14,<sup>39</sup> were found to have opposite trends in behavior based on concentration and temperature; Labrasol<sup>®</sup> microemulsions showed a decrease in the measured  $R_H$  (90 nm to 6 nm) with increased concentration, while Gelucire<sup>®</sup> 44/14 showed an increase in measured  $R_H$  (1 nm to 5.5 nm) with increased concentration. The authors postulate that this opposite trend was due to coacervation in low concentrations of Labrasol<sup>®</sup> and increase in viscosity of higher concentrations of Gelucire<sup>®</sup> 44/14.

An often-important criteria for drug delivery systems is the ability to keep the loaded drug inside the prepared emulsion or droplet solution in the gastrointestinal tract, where digestive enzymes are present. In continuation of their previous studies, Chamieh *et al.* monitored the size of excipients during *in vitro* lipolysis under conditions simulating the gastrointestinal tract.<sup>41</sup> Digestion of the excipients were monitored by TDA at several time points in the degradation process. Similar to their previous work, an opposite behavior was observed, as Labrasol<sup>®</sup> droplets decrease in size (Figs. 6A and 6B), due to the disappearance of coacervates that are unable to solubilize the hydrophobic fluorescent marker and Gelucire<sup>®</sup> droplets increase in size during lipolysis (Figs. 6C and 6D) due to the increase in micelle size, maintaining solubilizing capacity. TDA was shown to be effective for size analysis of microemulsions and their behavior under digestive conditions. TDA is also an effective method for quantifying peptide

1  
2  
3 drugs released from lipidic self-emulsifying drug delivery systems. The role of electrolyte  
4 ionic strength on the release of two therapeutic peptides, leuprorelin and desmopressin  
5 has also been characterized.<sup>26</sup>  
6

## 7 TDA APPLICATIONS IN NANOMATERIALS CHARACTERIZATION

8  
9  
10 Physicochemical properties of inorganic nanoparticles (NPs) are primarily  
11 dependent on their size, and TDA has proven well-suited for characterizing NPs. Sizing  
12 of NPs by TDA has been well-studied and has demonstrated utility.<sup>43-51</sup> NP size  
13 characterization by TDA has been compared to TEM imaging techniques and found to  
14 result in comparable particle size values. For example, Balog *et al.* studied  
15 superparamagnetic iron oxide NPs (SPIONs), gold (Au) NPs, and silica (SiO<sub>2</sub>) NPs and  
16 compared TDA to TEM in determination of particle radius.<sup>43</sup> The reported radii of  
17 SPIONs, Au NPs, and SiO<sub>2</sub> NPs were 7.6 nm, 33.8 nm, and 44.0 nm, respectively, by  
18 TDA, and 6.7 ± 1.1 nm, 28.0 ± 4.7 nm, and 39.3 ± 6.2 nm, respectively, by TEM.  
19

20 Sizing is also useful in characterizing the modification of NPs with adsorbed  
21 functional components such as enzymes. Holdrich *et al.* investigated pepsin coated gold  
22 nanoparticles by DLS and TDA.<sup>47</sup> Pepsin was adsorbed onto synthesized gold  
23 nanoparticles (GNPs), with a DLS measured diameter of 44.1 ± 0.3 nm, at varying  
24 concentrations to obtain a range of thicknesses of the adsorbed layer. The average  
25 hydrodynamic diameter of pepsin-coated GNPs by DLS was reported as 64 ± 2 nm,  
26 where the GNPs synthesized with different concentrations of the pepsin coating solution  
27 were not significantly different. This suggests that DLS was unable to successfully  
28 distinguish the small differences in hydrodynamic diameter of the pepsin-GNP  
29 bioconjugates as compared to bare GNPs (Fig. 7A), while TDA successfully resolved  
30 increases in  $R_H$  due to pepsin adsorption as small as <2 nm with a high degree of  
31 repeatability and accuracy (Fig. 7B).  
32

33 Size characterization is also important for understanding organic materials, for  
34 observing polymer synthesis and degradation, ligand binding, and monitoring reaction  
35 progress. The utility of UV and fluorescence detection modes for TDA are discussed  
36 previously in this review. In many situations pertinent to organic synthesis, however,  
37 molecules may exhibit neither significant UV absorption nor fluorescence. Refractive  
38 index (RI) detection is a potential alternative in these cases, and RI detection has been  
39 used for TDA performed with HPLC instrumentation, but these examples required  
40 detection volumes on the order of 10 µL, which eliminates the key advantages of small  
41 sample volumes and reduced analysis times in TDA.<sup>62, 101, 102</sup> Saetear *et al.* developed a  
42 backscattering interferometry (BSI) approach to improve RI detection in TDA with  
43 nanoliter sample volumes.<sup>89</sup> A selection of poly- and monosaccharides, which present a  
44 significant detection challenge due to low UV absorbance, were characterized by TDA  
45 using the BSI technique in a commercial CE instrument. Determinations of  $D$  gave an  
46 average RSD of 2%, demonstrating high repeatability in the TDA-BSI analyses of non-  
47 UV absorbing molecules. In continuation of this study, Leclercq *et al.* investigated a UV-  
48 photooxidation (UV-POD) detection mode for TDA of polysaccharides and compared  
49 results to the BSI method, as detection sensitivity of TDA-BSI is relatively low (LOD ≈  
50 50 – 80 mg L<sup>-1</sup>).<sup>22</sup>  $R_H$  values for a selection of polysaccharides were determined by  
51 TDA-BSI and TDA-UV-POD with an average relative difference in  $R_H$  between the two  
52  
53  
54  
55  
56  
57  
58  
59  
60

1  
2  
3 detection modes of ~2% and an RSD below 3%. Additionally, detection sensitivity of  
4 TDA-UV-POD for pullulans and dextrans was greater than that of TDA-BSI (LOD = 40  
5 mg L<sup>-1</sup> and 50 – 60 mg L<sup>-1</sup>, respectively). These works expand the applications of TDA  
6 to applications requiring universal detection modes.  
7

8 Characterizing the degradation products of biopolymers is essential for  
9 understanding the fate of these materials in biomedical applications. The application of  
10 TDA to monitoring hydrolytic degradation of a fifth generation dendrigraft poly-L-lysine  
11 (DGL G5) has been described.<sup>60</sup> Using three different approaches – curve fitting,  
12 cumulant series expansion, and constrained regularized linear inversion -  $R_H$  values  
13 were obtained at different degradation times. The  $R_H$  value for the enzymatic  
14 degradation of DGL  $n$  corresponds to the  $R_H$  of the  $n-1$  generation, elucidating structural  
15 and behavioral information about the polymer and enzyme, such as reaction kinetics  
16 and degradation process. Other biopolymers, such as natural rubber,<sup>103</sup> polyplexes,<sup>21</sup>  
17 and the influence of ionic strength<sup>104</sup> on these systems have also been studied by TDA.  
18  
19

## 20 CONCLUSION

21 In this review, we aimed to illustrate TDA as a powerful sizing technique that  
22 offers comparable sizing performance with reduced sample consumption and often  
23 improved detection sensitivity as compared to more common sizing techniques such as  
24 DLS, SEC, or various imaging approaches. First, we offered a tutorial on the  
25 fundamental principles that allow TDA to achieve calibration-free sizing of analytes  
26 across a wide range of  $R_H$ , with an emphasis on the reduced sample consumption and  
27 analysis times that result from utilizing fused silica capillaries. We continued by  
28 highlighting relationships between operating parameters, such as  $u$  and  $R_c$ , and the  
29 critically important Taylor conditions. Our intention was to acquaint those seeking to  
30 utilize TDA with the careful consideration needed to design effective TDA experiments.  
31 Our discussion continued by looking at methods for applying TDA to sample mixtures,  
32 first via algorithmic approaches, then by looking at the integration of CE and TDA.  
33 Finally, we presented a selection of reports that demonstrate TDA applied to complex  
34 challenges in bioanalysis and materials science.  
35  
36  
37

38 TDA is a particularly attractive analytical method because it achieves calibration-  
39 free sizing across an impressive dynamic range (ca. Å - μm) while utilizing nL sample  
40 volumes and straightforward and accessible instrumentation. We see a valuable  
41 opportunity to expand the adoption of this technology within the broader separation  
42 science community. Meeting that opportunity requires effort in a few areas. First, wider  
43 dissemination of the principles and capabilities of TDA are needed, towards which we  
44 offer the current tutorial review. Second, navigating the relationship between operating  
45 parameters and meeting the Taylor conditions is a barrier to entry for those with little or  
46 no prior experience in TDA. This barrier would be substantially lowered by making  
47 available adaptable, open-source calculation tools. Third, although TDA can be readily  
48 achieved with commercial CE instrumentation, the cost of these instruments is not  
49 trivial, and their capabilities far exceed the minimum requirements for typical TDA  
50 analysis. Therefore, those without a CE instrument may not be inclined to acquire one  
51 for the sole purpose of TDA, and those with a CE instrument may find its broader  
52 capabilities put to more efficient use for other purposes. A few TDA-specific instruments  
53 are commercially available, but the cost may be yet another barrier to entry. Ultimately,  
54  
55  
56  
57  
58  
59  
60

1  
2  
3 TDA is a mechanistically simple measurement to implement, which may be amenable to  
4 the development of low-cost, open-source hardware that will enable wide adoption of  
5 this powerful analytical method. We believe that wider adoption of TDA will enable new  
6 dimensions of analysis across various sub-fields of analytical chemistry and  
7 measurement science.  
8  
9

### 10 **CONFLICTS OF INTEREST**

11 There are no conflicts of interest to declare.  
12

### 13 **ACKNOWLEDGEMENTS**

14 The authors were supported by funds from the National Institute of General  
15 Medical Sciences of the National Institutes of Health under award number  
16 R35GM138173.  
17  
18  
19  
20  
21  
22  
23  
24  
25  
26  
27  
28  
29  
30  
31  
32  
33  
34  
35  
36  
37  
38  
39  
40  
41  
42  
43  
44  
45  
46  
47  
48  
49  
50  
51  
52  
53  
54  
55  
56  
57  
58  
59  
60

**Fig. 1** Illustration of Taylor dispersion, and the corresponding variables utilized in TDA. Under the parabolic velocity profile of pressure-driven flow, and neglecting any effects of diffusion, a sample plug would deform as illustrated (i). Considering the effects of diffusion only in the radial direction gives Taylor dispersion, yielding the band profiles illustrated (ii). The evolution of Taylor dispersion can be observed as band broadening of a peak measured at multiple locations in the flow path (iii). The variables  $t_1$ ,  $t_2$ ,  $R_c$ ,  $\sigma_1$ , and  $\sigma_2$  are the same variables utilized in Equation 13.

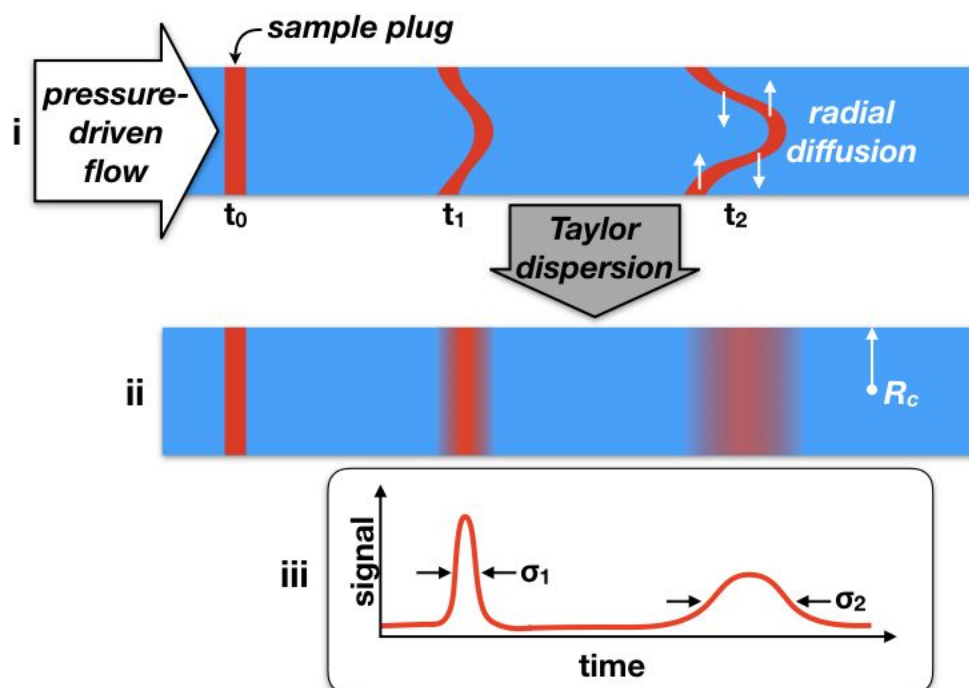


**Fig. 2** Illustration of the conditions under which HDC mechanisms interfere with the accurate interpretation of TDA results for A) 50  $\mu\text{m}$  i.d. and B) 25  $\mu\text{m}$  i.d. capillaries. Red lines correspond to experimental conditions of constant analyte size (vertical) or constant mobilizing pressure (horizontal), and the dots represent experimental conditions investigated. Taylorgrams obtained from PS NPs with C) constant analyte size at various mobilizing pressures and D) constant mobilizing pressure with various analyte sizes. Note that deviations from gaussian peak shape arise when experimental conditions enter the HDC regime, illustrated as shaded green region in A and B.

Adapted with permission from: Chamieh J, Leclercq L, Martin M, Slaoui S, Jensen H, Ostergaard J, et al. Limits in Size of Taylor Dispersion Analysis: Representation of the Different Hydrodynamic Regimes and Application to the Size-Characterization of Cubosomes. *Anal Chem.* 2017; 89(24):13487-93. Copyright (2017) American Chemical Society.

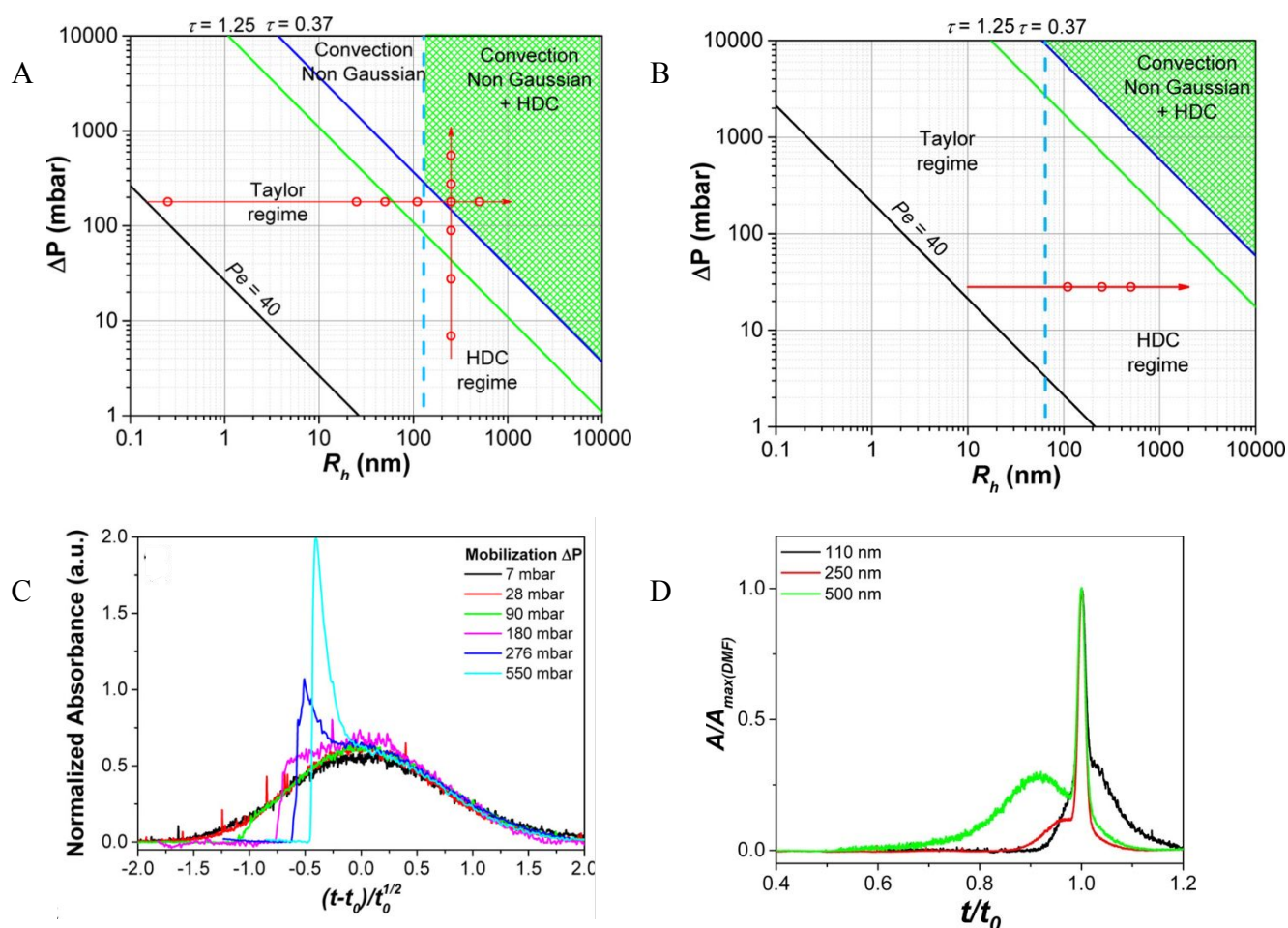


**Fig. 3** Graphical representation of variance determination by peak integration. A) Integration boundaries are represented by cut-off lines given as percentage of the peak apex (horizontal dashed lines); and B) resulting trends in  $R_H$  measurements as a function of integration cut-off boundaries. The limiting cut-off boundary was determined to be 0.75% (vertical dashed line), which represented  $4 \times \sigma_{noise}$ .  $R_H$  measurements by the integration method (data points) are compared to standard gaussian peak fitting values (horizontal dashed lines). Reprinted from *Journal of Chromatography A*, Vol. 1241, Joseph Chamieh, Herve Cottet, Comparison of single and double detection points Taylor Dispersion Analysis for monodisperse and polydisperse samples, 123-127, Copyright (2012), with permission from Elsevier.

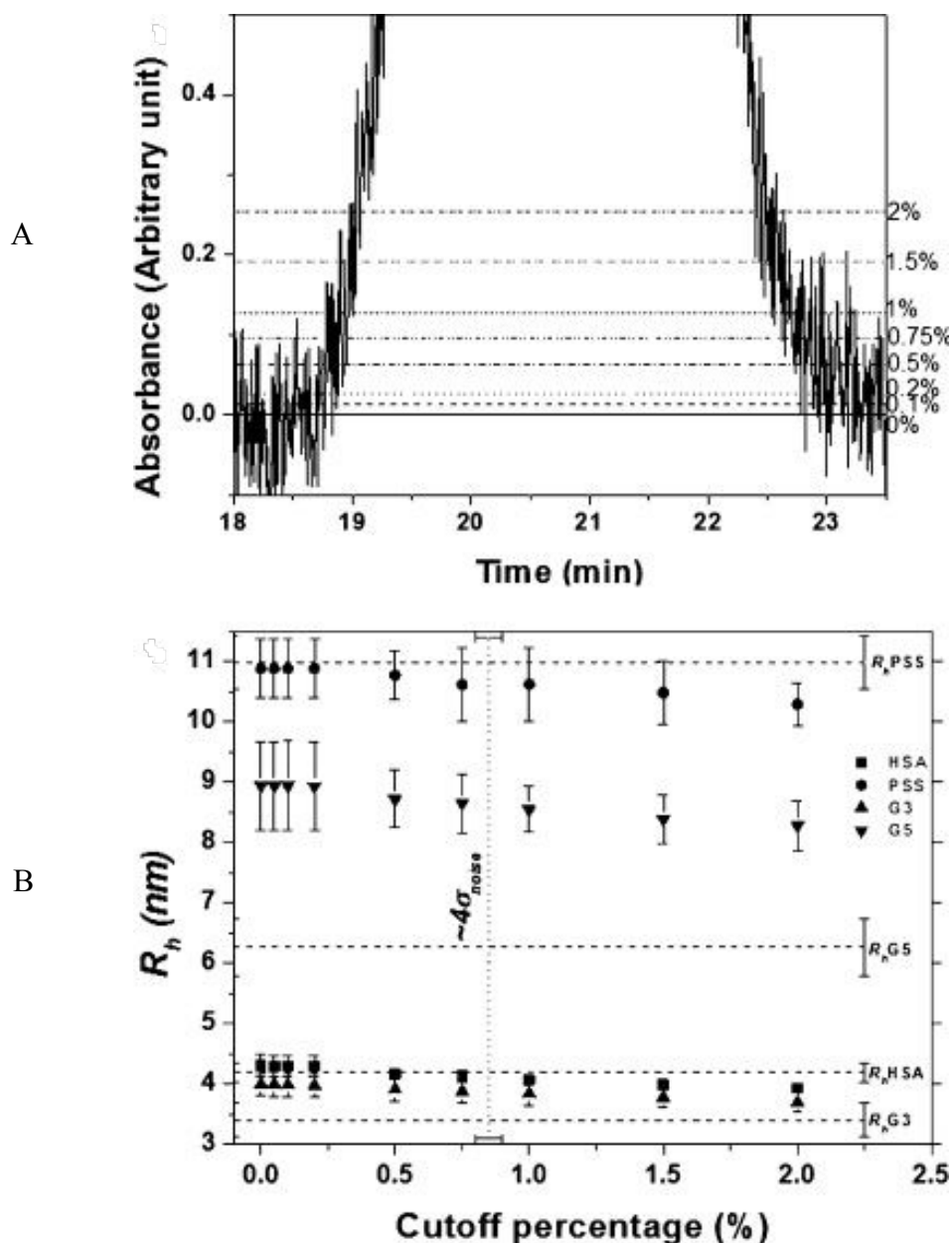
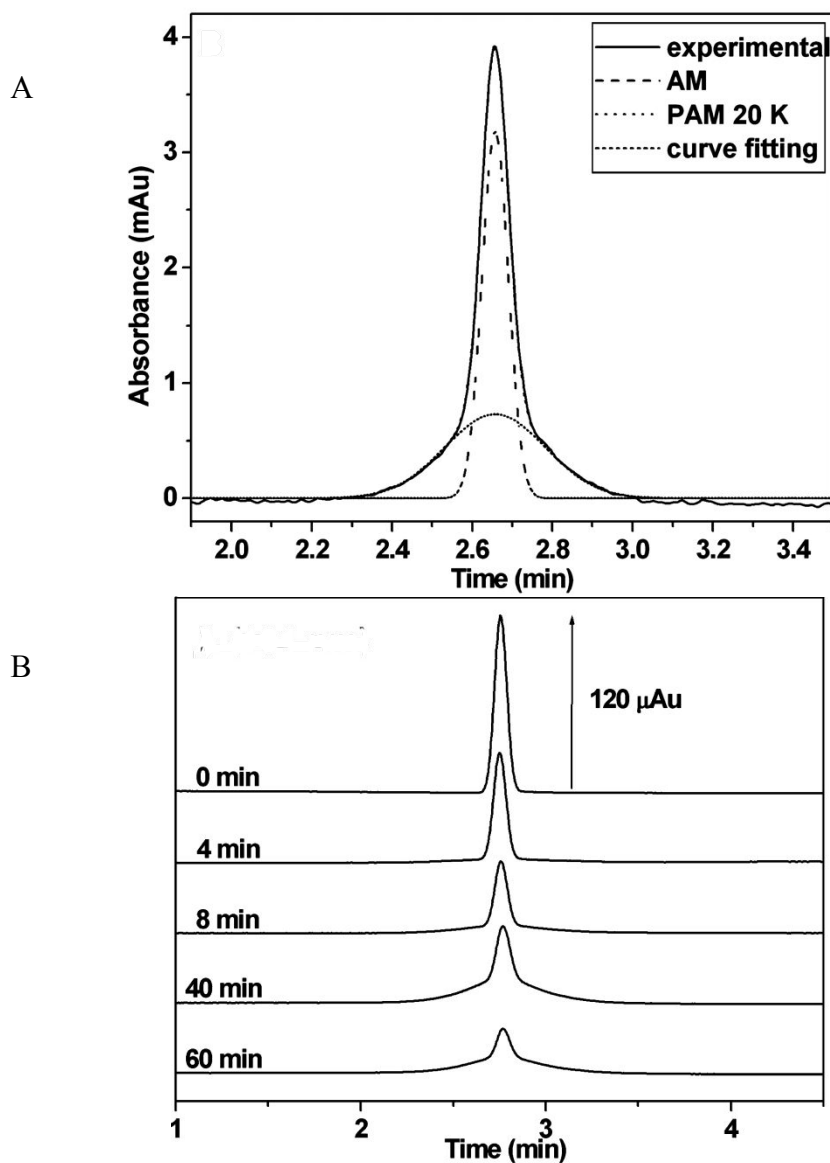


**Fig. 4** A) Taylorgram of an AM/PAM standard mixture with UV absorbance detection (solid line). The signal was deconvoluted by fitting to the sum of two gaussian curves (dashed lines) . B) TDA time course profile of acrylamide polymerization with UV absorbance detection at 191 nm. Signal analysis using three methods based on conservation of mass of sample injection, deconvolution via gaussian fits, and deconvolution via monomer contribution subtraction results in  $R_H$  determinations that agree to within 4%. Adapted with permission from: Cottet H, Biron JP, Cipelletti L, Matmour R, Martin M. Determination of Individual Diffusion Coefficients in Evolving Binary Mixtures by Taylor Dispersion Analysis: Application to the Monitoring of Polymer Reaction. Anal Chem. 2010; 82(5):1793-802. Copyright (2010) American Chemical Society.





1  
2  
3 **Fig. 5** A) Illustration of a looped capillary within a standard CE instrument cassette for  
4 double detection TDA with UV absorbance detection. B) Raw data (top) and normalized  
5 data (bottom) taylorgrams of HSA by conventional single-point UV absorbance  
6 detection interface (gray trace) and modified double detection interface (black trace).  
7 Note a dramatic reduction in sensitivity (ca. 10-fold) for the modified double detection  
8 interface. Normalized data shows no substantial difference in peak variance or elution  
9 time between detection methods. Adapted from Journal of Chromatography A, Vol.  
10 1235, Joseph Chamieh, Farid Oukacine, Herve Cottet, Taylor dispersion analysis with  
11 two detection points on a commercial capillary electrophoresis apparatus, 174-177,  
12 Copyright (2012), with permission from Elsevier. C) Schematic illustration and  
13 photograph (scale bar is 5 mm) of a miniature 3D printed fluorescence detector for two-  
14 point fluorescence detection in a commercial CE instrument. D) Raw (top) and  
15 Gaussian fitted (bottom) data from CE-TDA of FITC-BSA conjugation reaction. TDA  
16 determinations of  $R_H$  enabled peak assignments of FITC-BSA (first peak) and free FITC  
17 (second peak). Adapted with permission from: Casto LD, Do KB, Baker CA. A Miniature 3D Printed LED-  
18 Induced Fluorescence Detector for Capillary Electrophoresis and Dual-Detector Taylor Dispersion Analysis. Anal Chem. 2019;  
19 91(15):9451-7. Copyright (2019) American Chemical Society.  
20  
21  
22  
23  
24  
25  
26  
27  
28  
29  
30  
31  
32  
33  
34  
35  
36  
37  
38  
39  
40  
41  
42  
43  
44  
45  
46  
47  
48  
49  
50  
51  
52  
53  
54  
55  
56  
57  
58  
59  
60

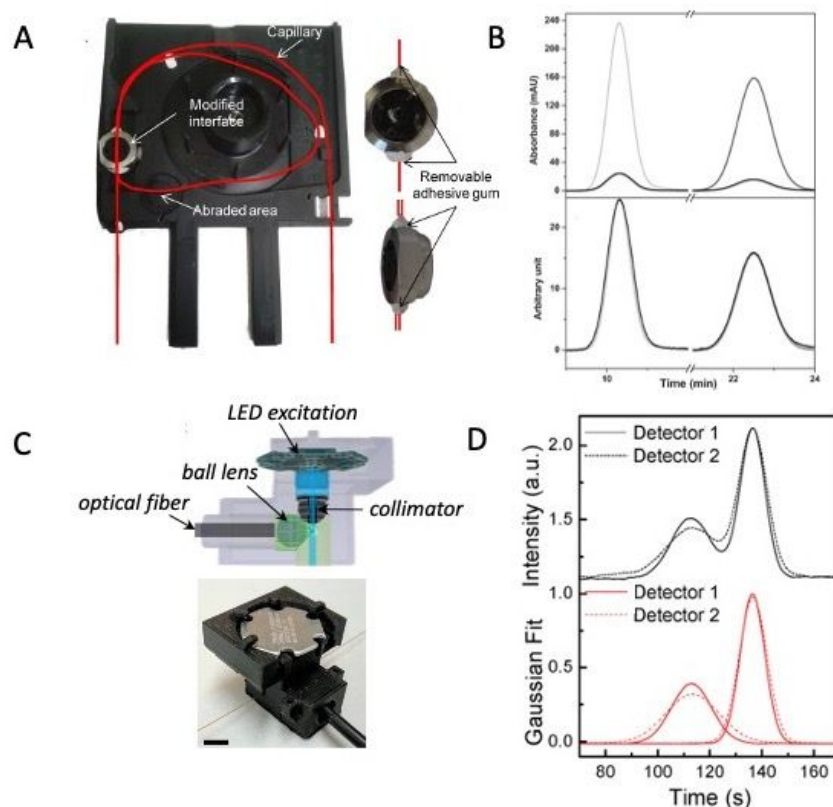


**Fig. 6** Graphical comparison of diffusion coefficients and hydrodynamic radii of Labrasol® and Gelucire® droplets during lipolysis at 37°C. A)  $D$  measurements of Labrasol® droplets are shown to increase and B) corresponding  $R_H$  values decrease exponentially before reaching a plateau. C)  $D$  measurements of Gelucire® droplets are shown to decrease and D) corresponding  $R_H$  values increase sigmoidally. Adapted from International Journal of Pharmaceutics, Vol. 537, Joseph Chamieh, Habib Merdassi, Jean-Christophe Rossi, Vincent Jannin, Frederic Demarne, Herve Cottet, Size characterization of lipid-based self-emulsifying pharmaceutical excipients during lipolysis using Taylor dispersion analysis with fluorescence detection, 94-101, Copyright (2018), with permission from Elsevier.

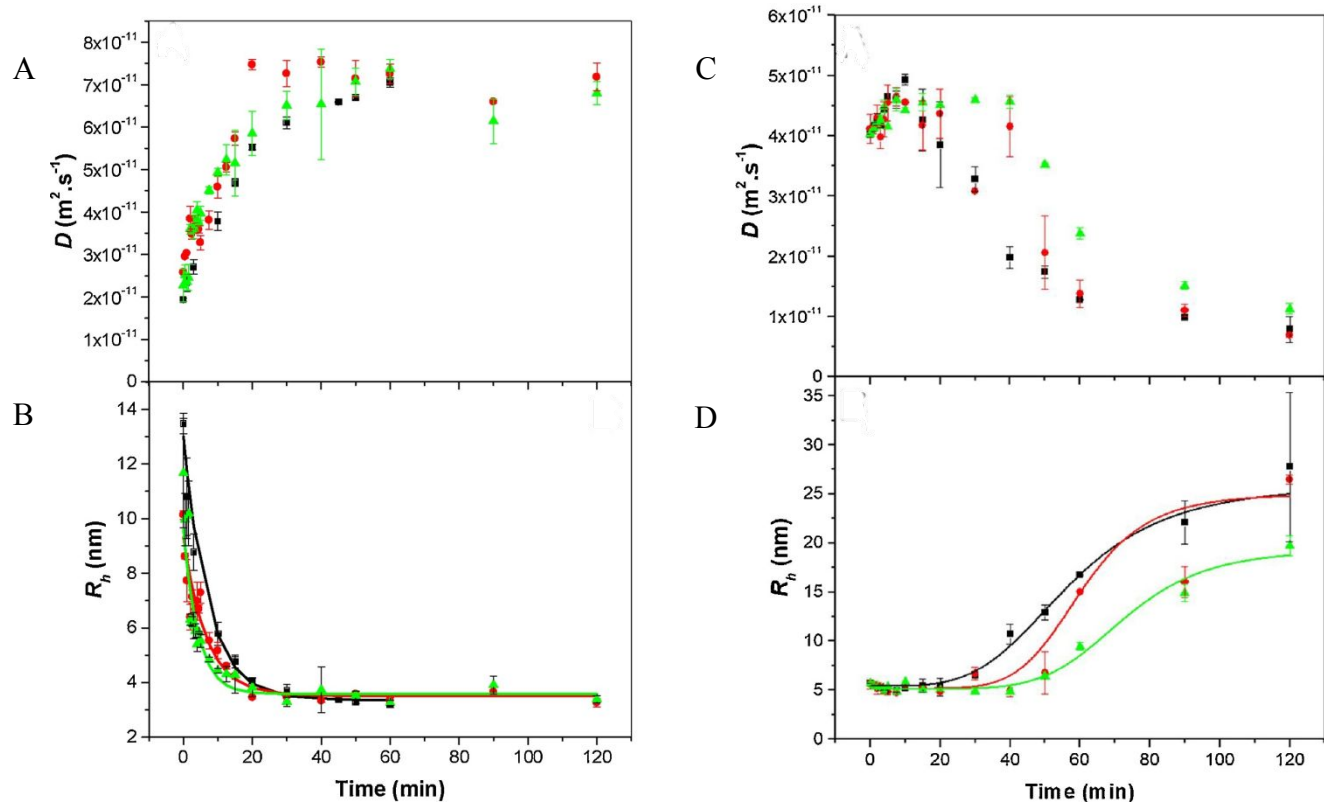
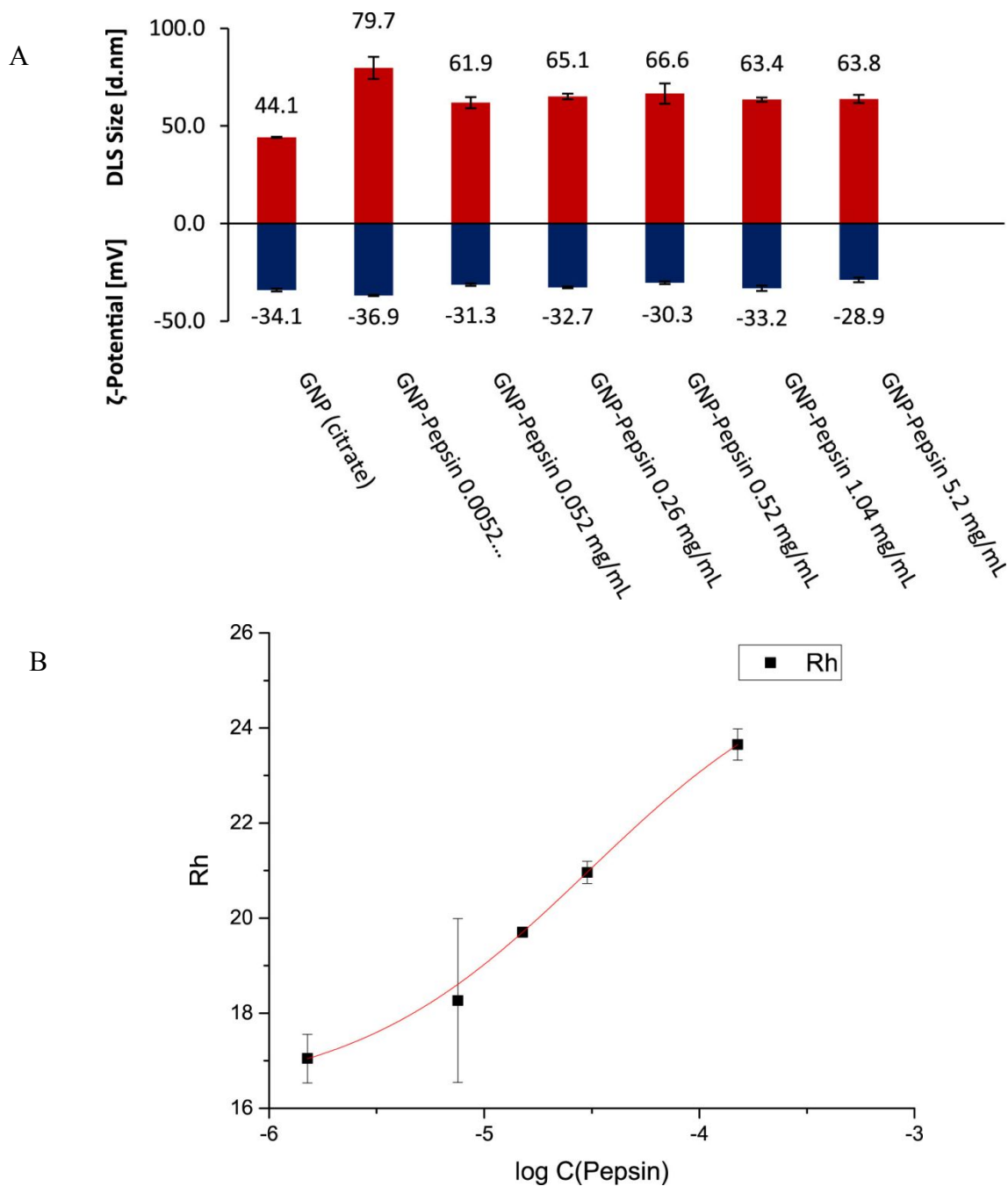


**Fig. 7** Comparison of A) DLS measurements for hydrodynamic diameters and B) TDA measurements for  $R_H$  of pepsin-coated GNPs at varying concentrations of pepsin. While increasing diameter of pepsin-functionalized GNPs was expected with increasing pepsin concentration, DLS did not resolve the small size differences of bioconjugates prepared at various pepsin concentrations. TDA resolved the trend of increasing  $R_H$  with increasing pepsin concentration. Adapted from Talanta, Vol. 167, Markus Holdrich, Siyao Liu, Markus Epe, Michael Lammerhofer, Taylor dispersion analysis, resonant mass measurement and bioactivity of pepsin-coated gold nanoparticles, 67-74, Copyright (2017), with permission from Elsevier.



## REFERENCES

1. Lawrie AS, Albanyan A, Cardigan RA, Mackie IJ, Harrison P. Microparticle sizing by dynamic light scattering in fresh-frozen plasma. *Vox Sang*. 2009;96(3):206-12.
2. Chaikov LL, Kirichenko MN, Krivokhizha SV, Zaritskiy AR. Dynamics of statistically confident particle sizes and concentrations in blood plasma obtained by the dynamic light scattering method. *J Biomed Opt*. 2015;20(5):7.
3. Stetefeld J, McKenna SA, Patel TR. Dynamic light scattering: a practical guide and applications in biomedical sciences. *Biophysical Reviews*. 2016;8(4):409-27.
4. Hawe A, Hulse WL, Jiskoot W, Forbes RT. Taylor Dispersion Analysis Compared to Dynamic Light Scattering for the Size Analysis of Therapeutic Peptides and Proteins and Their Aggregates. *Pharm Res*. 2011;28(9):2302-10.
5. Arakawa T, Ejima D, Li TS, Phil JS. The Critical Role of Mobile Phase Composition in Size Exclusion Chromatography of Protein Pharmaceuticals. *J Pharm Sci*. 2010;99(4):1674-92.
6. Pacakova V, Stulik K, Hau PT, Jelinek I, Vins I, Sykora D. COMPARISON OF HIGH-PERFORMANCE LIQUID-CHROMATOGRAPHY AND CAPILLARY ELECTROPHORESIS FOR THE DETERMINATION OF SOME BEE VENOM COMPONENTS. *J Chromatogr A*. 1995;700(1-2):187-93.
7. Ricker RD, Sandoval LA. Fast, reproducible size-exclusion chromatography of biological macromolecules. *J Chromatogr A*. 1996;743(1):43-50.
8. Bootz A, Vogel V, Schubert D, Kreuter J. Comparison of scanning electron microscopy, dynamic light scattering and analytical ultracentrifugation for the sizing of poly(butyl cyanoacrylate) nanoparticles. *Eur J Pharm Biopharm*. 2004;57(2):369-75.
9. Hegel C, Jones C, Cabrera F, Yanez MJ, Bucala V. PARTICLE SIZE CHARACTERIZATION: COMPARISON OF LASER DIFRACTION (LD) AND SCANNING ELECTRON MICROSCOPY (SEM). *Acta Microsc*. 2014;23(1):11-7.
10. Sokolova V, Ludwig AK, Hornung S, Rotan O, Horn PA, Epple M, et al. Characterisation of exosomes derived from human cells by nanoparticle tracking analysis and scanning electron microscopy. *Colloid Surf B-Biointerfaces*. 2011;87(1):146-50.
11. Haiss W, Thanh NTK, Aveyard J, Fernig DG. Determination of size and concentration of gold nanoparticles from UV-Vis spectra. *Anal Chem*. 2007;79(11):4215-21.
12. Wang ZL. Transmission electron microscopy of shape-controlled nanocrystals and their assemblies. *J Phys Chem B*. 2000;104(6):1153-75.
13. Garcia R, Perez R. Dynamic atomic force microscopy methods. *Surf Sci Rep*. 2002;47(6-8):197-301.
14. Grobelny J, DelRio FW, Pradeep N, Kim DI, Hackley VA, Cook RF. Size Measurement of Nanoparticles Using Atomic Force Microscopy. In: McNeil SE, editor. *Characterization of Nanoparticles Intended for Drug Delivery*. Methods in Molecular Biology. 697. Totowa: Humana Press Inc; 2011. p. 71-82.
15. Cottet H, Biron JP, Martin M. Taylor dispersion Analysis of mixtures. *Anal Chem*. 2007;79(23):9066-73.

16. Casto LD, Do KB, Baker CA. A Miniature 3D Printed LED-Induced Fluorescence Detector for Capillary Electrophoresis and Dual-Detector Taylor Dispersion Analysis. *Anal Chem.* 2019;91(15):9451-7.
17. Chamieh J, Oukacine F, Cottet H. Taylor dispersion analysis with two detection points on a commercial capillary electrophoresis apparatus. *J Chromatogr A.* 2012;1235:174-7.
18. Latunde-Dada S, Bott R, Barker D, Leszczyszyn OI. Methodologies for the rapid determination of the diffusion interaction parameter using Taylor dispersion analysis. *Analytical Methods.* 2016;8(2):386-92.
19. Secuianu C, Maitland GC, Trusler JPM, Wakeham WA. Mutual Diffusion Coefficients of Aqueous KCl at High Pressures Measured by the Taylor Dispersion Method. *Journal of Chemical and Engineering Data.* 2011;56(12):4840-8.
20. Zhuang GS, Poulsen NN, Petersen NJ, Ostergaard J, Jensen H, Ieee. A Capillary-based Microfluidic Device Incorporating Optical Fibers for Flow Induced Dispersion Analysis 2013. 1054-7 p.
21. Leclercq L, Reinhard S, Chamieh J, Doblinger M, Wagner E, Cottet H. Fast Characterization of Polyplexes by Taylor Dispersion Analysis. *Macromolecules.* 2015;48(19):7216-21.
22. Leclercq L, Saetear P, Rolland-Sabate A, Biron JP, Chamieh J, Cipelletti L, et al. Size-Based Characterization of Polysaccharides by Taylor Dispersion Analysis with Photochemical Oxidation or Backscattering Interferometry Detections. *Macromolecules.* 2019;52(12):4421-31.
23. Taylor G. Dispersion of Soluble Matter in Solvent Flowing Slowly Through a Tube. *Proc Royal Soc London.* 1953;219(1137):186-203.
24. Taylor G. THE DISPERSION OF MATTER IN TURBULENT FLOW THROUGH A PIPE. *Proceedings of the Royal Society of London Series a-Mathematical and Physical Sciences.* 1954;223(1155):446-68.
25. Giddings JC, Seager SL. RAPID DETERMINATION OF GASEOUS DIFFUSION COEFFICIENTS BY MEANS OF GAS CHROMATOGRAPHY APPARATUS. *J Chem Phys.* 1960;33(5):1579-80.
26. Chamieh J, Tarrat AD, Doudou C, Jannin V, Demarne F, Cottet H. Peptide release from SEDDS containing hydrophobic ion pair therapeutic peptides measured by Taylor dispersion analysis. *International Journal of Pharmaceutics.* 2019;559:228-34.
27. Hogstedt UB, Schwach G, van de Weert M, Ostergaard J. Taylor Dispersion Analysis as a promising tool for assessment of peptide-peptide interactions. *European Journal of Pharmaceutical Sciences.* 2016;93:21-8.
28. Hulse W, Forbes R. A Taylor dispersion analysis method for the sizing of therapeutic proteins and their aggregates using nanolitre sample quantities. *International Journal of Pharmaceutics.* 2011;416(1):394-7.
29. Hulse WL, Gray J, Forbes RT. Evaluating the inter and intra batch variability of protein aggregation behaviour using Taylor dispersion analysis and dynamic light scattering. *International Journal of Pharmaceutics.* 2013;453(2):351-7.
30. Ibrahim A, Meyrueix R, Pouliquen G, Chan YP, Cottet H. Size and charge characterization of polymeric drug delivery systems by Taylor dispersion analysis and capillary electrophoresis. *Analytical and Bioanalytical Chemistry.* 2013;405(16):5369-79.

- 1  
2  
3 31. Jensen SS, Jensen H, Cornett C, Moller EH, Ostergaard J. Insulin diffusion and  
4 self-association characterized by real-time UV imaging and Taylor dispersion analysis.  
5 *Journal of Pharmaceutical and Biomedical Analysis*. 2014;92:203-10.
- 6 32. Lavoisier A, Schlaeppli JM. Early developability screen of therapeutic antibody  
7 candidates using Taylor dispersion analysis and UV area imaging detection. *Mabs*.  
8 2015;7(1):77-83.
- 9 33. Poulsen NN, Andersen NZ, Ostergaard J, Zhuang GS, Petersen NJ, Jensen H.  
10 Flow induced dispersion analysis rapidly quantifies proteins in human plasma samples.  
11 *Analyst*. 2015;140(13):4365-9.
- 12 34. Poulsen NN, Pedersen ME, Ostergaard J, Petersen NJ, Nielsen CT, Heegaard  
13 NHH, et al. Flow-Induced Dispersion Analysis for Probing Anti-dsDNA Antibody Binding  
14 Heterogeneity in Systemic Lupus Erythematosus Patients: Toward a New Approach for  
15 Diagnosis and Patient Stratification. *Anal Chem*. 2016;88(18):9056-61.
- 16 35. Zuo M, Chen Y. Fast determination of protein diffusion coefficient by Taylor  
17 dispersion analysis and capillary electrophoresis system. *Chemical Journal of Chinese*  
18 *Universities-Chinese*. 2007;28(10):1875-7.
- 19 36. Restan MS, Pedersen ME, Jensen H, Pedersen-Bjergaard S. Electromembrane  
20 Extraction of Unconjugated Fluorescein Isothiocyanate from Solutions of Labeled  
21 Proteins Prior to Flow Induced Dispersion Analysis. *Anal Chem*. 2019;91(10):6702-8.
- 22 37. Ye FB, Jensen H, Larsen SW, Yaghmur A, Larsen C, Ostergaard J.  
23 Measurement of drug diffusivities in pharmaceutical solvents using Taylor dispersion  
24 analysis. *Journal of Pharmaceutical and Biomedical Analysis*. 2012;61:176-83.
- 25 38. Zaman H, Bright AG, Adams K, Goodall DM, Forbes RT. Characterisation of  
26 aggregates of cyclodextrin-drug complexes using Taylor Dispersion Analysis.  
27 *International Journal of Pharmaceutics*. 2017;522(1-2):98-109.
- 28 39. Chamieh J, Davanier F, Jannin V, Demarne F, Cottet H. Size characterization of  
29 commercial micelles and microemulsions by Taylor dispersion analysis. *International*  
30 *Journal of Pharmaceutics*. 2015;492(1-2):46-54.
- 31 40. Chamieh J, Jannin V, Demarne F, Cottet H. Hydrodynamic size characterization  
32 of a self-emulsifying lipid pharmaceutical excipient by Taylor dispersion analysis with  
33 fluorescent detection. *International Journal of Pharmaceutics*. 2016;513(1-2):262-9.
- 34 41. Chamieh J, Merdassi H, Rossi JC, Jannin V, Demarne F, Cottet H. Size  
35 characterization of lipid-based self-emulsifying pharmaceutical excipients during  
36 lipolysis using Taylor dispersion analysis with fluorescence detection. *International*  
37 *Journal of Pharmaceutics*. 2018;537(1-2):94-101.
- 38 42. Petr J. Rapid determination of the critical micelle concentration by Taylor  
39 dispersion analysis in capillaries using both direct and indirect detection. *Journal of*  
40 *Separation Science*. 2017;40(6):1421-6.
- 41 43. Balog S, Urban DA, Milosevic AM, Crippa F, Rothen-Rutishauser B, Petri-Fink A.  
42 Taylor dispersion of nanoparticles. *J Nanopart Res*. 2017;19(8).
- 43 44. Cipelletti L, Biron JP, Martin M, Cottet H. Measuring Arbitrary Diffusion  
44 Coefficient Distributions of Nano-Objects by Taylor Dispersion Analysis. *Anal Chem*.  
45 2015;87(16):8489-96.
- 46 45. d'Orlye F, Varenne A, Gareil P. Determination of nanoparticle diffusion  
47 coefficients by Taylor dispersion analysis using a capillary electrophoresis instrument. *J*  
48 *Chromatogr A*. 2008;1204(2):226-32.
- 49  
50  
51  
52  
53  
54  
55  
56  
57  
58  
59  
60

- 1
- 2
- 3
- 4 46. Hajiani P, Larachi F. Reducing Taylor dispersion in capillary laminar flows using
- 5 magnetically excited nanoparticles: Nanomixing mechanism for micro/nanoscale
- 6 applications. *Chemical Engineering Journal*. 2012;203:492-8.
- 7 47. Holdrich M, Liu SY, Epe M, Lammerhofer M. Taylor dispersion analysis, resonant
- 8 mass measurement and bioactivity of pepsin-coated gold nanoparticles. *Talanta*.
- 9 2017;167:67-74.
- 10 48. Lemal P, Petri-Fink A, Balog S. Nanoparticles and Taylor Dispersion as a Linear
- 11 Time-Invariant System. *Anal Chem*. 2019;91(2):1217-21.
- 12 49. Pyell U, Jalil AH, Pfeiffer C, Pelaz B, Parak WJ. Characterization of gold
- 13 nanoparticles with different hydrophilic coatings via capillary electrophoresis and Taylor
- 14 dispersion analysis. Part I: Determination of the zeta potential employing a modified
- 15 analytic approximation. *J Colloid Interface Sci*. 2015;450:288-300.
- 16 50. Pyell U, Jalil AH, Urban DA, Pfeiffer C, Pelaz B, Parak WJ. Characterization of
- 17 hydrophilic coated gold nanoparticles via capillary electrophoresis and Taylor dispersion
- 18 analysis. Part II: Determination of the hydrodynamic radius distribution - Comparison
- 19 with asymmetric flow field-flow fractionation. *J Colloid Interface Sci*. 2015;457:131-40.
- 20 51. Urban DA, Milosevic AM, Bossert D, Crippa F, Moore TL, Geers C, et al. Taylor
- 21 Dispersion of Inorganic Nanoparticles and Comparison to Dynamic Light Scattering and
- 22 Transmission Electron Microscopy. *Colloid and Interface Science Communications*.
- 23 2018;22:29-33.
- 24 52. Li ZQ, Wu ZQ, Xia XH. Study of Interaction of Nanoparticles and Proteins in
- 25 Taylor Dispersion Analysis. *Chinese Journal of Analytical Chemistry*. 2017;45(12):1980-
- 26 7.
- 27 53. Chamieh J, Cottet H. Comparison of single and double detection points Taylor
- 28 Dispersion Analysis for monodisperse and polydisperse samples. *J Chromatogr A*.
- 29 2012;1241:123-7.
- 30 54. Cipelletti L, Biron JP, Martin M, Cottet H. Polydispersity Analysis of Taylor
- 31 Dispersion Data: The Cumulant Method. *Anal Chem*. 2014;86(13):6471-8.
- 32 55. Cottet H, Biron JP, Cipelletti L, Matmour R, Martin M. Determination of Individual
- 33 Diffusion Coefficients in Evolving Binary Mixtures by Taylor Dispersion Analysis:
- 34 Application to the Monitoring of Polymer Reaction. *Anal Chem*. 2010;82(5):1793-802.
- 35 56. Cottet H, Biron JP, Martin M. On the optimization of operating conditions for
- 36 Taylor dispersion analysis of mixtures. *Analyst*. 2014;139(14):3552-62.
- 37 57. Latunde-Dada S, Bott R, Hampton K, Patel J, Leszczyszyn OI. Methodologies for
- 38 the Taylor dispersion analysis for mixtures, aggregates and the mitigation of buffer
- 39 mismatch effects. *Analytical Methods*. 2015;7(24):10312-21.
- 40 58. Price WE. THEORY OF THE TAYLOR DISPERSION TECHNIQUE FOR 3-
- 41 COMPONENT-SYSTEM DIFFUSION MEASUREMENTS. *Journal of the Chemical*
- 42 *Society-Faraday Transactions I*. 1988;84:2431-9.
- 43 59. Steuer W, Jost K, Halasz I. AVERAGED MOLECULAR-WEIGHT OF COMPLEX-
- 44 MIXTURES AS DETERMINED BY RAPID MEASUREMENTS OF DIFFUSION.
- 45 *Chromatographia*. 1985;20(1):13-9.
- 46 60. Chamieh J, Biron JP, Cipelletti L, Cottet H. Monitoring Biopolymer Degradation
- 47 by Taylor Dispersion Analysis. *Biomacromolecules*. 2015;16(12):3945-51.
- 48 61. Horvath J, Dolnik V. Polymer wall coatings for capillary electrophoresis.
- 49 *Electrophoresis*. 2001;22(4):644-55.
- 50
- 51
- 52
- 53
- 54
- 55
- 56
- 57
- 58
- 59
- 60

- 1
- 2
- 3
- 4 62. Kelly B, Leaist DG. Using Taylor dispersion profiles to characterize polymer
- 5 molecular weight distributions. *Phys Chem Chem Phys*. 2004;6(24):5523-30.
- 6 63. Boyle WA, Buchholz RF, Neal JA, McCarthy JL. FLOW-INJECTION ANALYSIS
- 7 ESTIMATION OF DIFFUSION-COEFFICIENTS OF PAUCIDISPERSE AND
- 8 POLYDISPERSE POLYMERS SUCH AS POLYSTYRENE SULFONATES. *J Appl*
- 9 *Polym Sci*. 1991;42(7):1969-77.
- 10 64. Cottet H, Martin M, Papillaud A, Souaid E, Collet H, Commeyras A.
- 11 Determination of dendrigraft poly-L-lysine diffusion coefficients by Taylor dispersion
- 12 analysis. *Biomacromolecules*. 2007;8(10):3235-43.
- 13 65. Franzen U, Ostergaard J. Physico-chemical characterization of liposomes and
- 14 drug substance-liposome interactions in pharmaceuticals using capillary electrophoresis
- 15 and electrokinetic chromatography. *J Chromatogr A*. 2012;1267:32-44.
- 16 66. Jensen H, Larsen SW, Larsen C, Ostergaard J. Physicochemical profiling of drug
- 17 candidates using capillary-based techniques. *J Drug Deliv Sci Technol*. 2013;23(4):333-
- 18 45.
- 19 67. Khodabandehloo A, Chen DD. Particle sizing methods for the detection of protein
- 20 aggregates in biopharmaceuticals. *Bioanalysis*. 2017;9(3):313-26.
- 21 68. Song HY, Cabooter D. Relevance and Assessment of Molecular Diffusion
- 22 Coefficients in Liquid Chromatography. *Chromatographia*. 2017;80(5):651-63.
- 23 69. Feng SL, Shirani E, Inglis DW. Droplets for Sampling and Transport of Chemical
- 24 Signals in Biosensing: A Review. *Biosensors-Basel*. 2019;9(2):14.
- 25 70. Liu SY, Lammerhofer M. Functionalized gold nanoparticles for sample
- 26 preparation: A review. *Electrophoresis*. 2019;40(18-19):2438-61.
- 27 71. Aris R. ON THE DISPERSION OF A SOLUTE IN A FLUID FLOWING
- 28 THROUGH A TUBE. *Proceedings of the Royal Society of London Series a-*
- 29 *Mathematical and Physical Sciences*. 1956;235(1200):67-77.
- 30 72. Sharma U, Gleason NJ, Carbeck JD. Diffusivity of solutes measured in glass
- 31 capillaries using Taylor's analysis of dispersion and a commercial CE instrument. *Anal*
- 32 *Chem*. 2005;77(3):806-13.
- 33 73. Schaschke C. Stokes-Einstein Equation. *A Dictionary of Chemical Engineering:*
- 34 *Oxford University Press*; 2014.
- 35 74. Taylor G. CONDITIONS UNDER WHICH DISPERSION OF A SOLUTE IN A
- 36 STREAM OF SOLVENT CAN BE USED TO MEASURE MOLECULAR DIFFUSION.
- 37 *Proceedings of the Royal Society of London Series a-Mathematical and Physical*
- 38 *Sciences*. 1954;225(1163):473-7.
- 39 75. Latunde-Dada S, Bott R, Crozier J, Trikeriotis M, Leszczyszyn OI, Goodall D.
- 40 Rapid determination of hydrodynamic radii beyond the limits of Taylor dispersion. *J*
- 41 *Chromatogr A*. 2016;1472:66-73.
- 42 76. Ostergaard J, Jensen H. Simultaneous Evaluation of Ligand Binding Properties
- 43 and Protein Size by Electrophoresis and Taylor Dispersion in Capillaries. *Anal Chem*.
- 44 2009;81(20):8644-8.
- 45 77. Hulse WL, Forbes RT. A nanolitre method to determine the hydrodynamic radius
- 46 of proteins and small molecules by Taylor dispersion analysis. *International Journal of*
- 47 *Pharmaceutics*. 2011;411(1-2):64-8.
- 48
- 49
- 50
- 51
- 52
- 53
- 54
- 55
- 56
- 57
- 58
- 59
- 60



- 1
- 2
- 3
- 4 78. Oukacine F, Morel A, Desvignes I, Cottet H. Size-based characterization of
- 5 nanoparticle mixtures by the inline coupling of capillary electrophoresis to Taylor
- 6 dispersion analysis. *J Chromatogr A*. 2015;1426:220-5.
- 7 79. Williams BA, Vigh G. Determination of effective mobilities and chiral separation
- 8 selectivities from partially separated enantiomer peaks in a racemic mixture using
- 9 pressure mediated capillary electrophoresis. *Anal Chem*. 1997;69(21):4410-8.
- 10 80. Chamieh J, Leclercq L, Martin M, Slaoui S, Jensen H, Ostergaard J, et al. Limits
- 11 in Size of Taylor Dispersion Analysis: Representation of the Different Hydrodynamic
- 12 Regimes and Application to the Size-Characterization of Cubosomes. *Anal Chem*.
- 13 2017;89(24):13487-93.
- 14 81. Latunde-Dada S, Bott R, Hampton K, Leszczyszyn OI. Analytical mitigation of
- 15 solute-capillary interactions in double detection Taylor Dispersion Analysis. *J*
- 16 *Chromatogr A*. 2015;1408:255-60.
- 17 82. Parmar AS, Muschol M. Hydration and Hydrodynamic Interactions of Lysozyme:
- 18 Effects of Chaotropic versus Kosmotropic Ions. *Biophys J*. 2009;97(2):590-8.
- 19 83. Wilkins DK, Grimshaw SB, Receveur V, Dobson CM, Jones JA, Smith LJ.
- 20 Hydrodynamic radii of native and denatured proteins measured by pulse field gradient
- 21 NMR techniques. *Biochemistry*. 1999;38(50):16424-31.
- 22 84. Wehr T, RodriguezDiaz R, Liu CM. Capillary electrophoresis of proteins. In:
- 23 Brown PR, Grushka E, editors. *Advances in Chromatography, Vol 37. Advances in*
- 24 *Chromatography*. 37. New York: Marcel Dekker; 1997. p. 237-361.
- 25 85. Doherty EAS, Meagher RJ, Albarghouthi MN, Barron AE. Microchannel wall
- 26 coatings for protein separations by capillary and chip electrophoresis. *Electrophoresis*.
- 27 2003;24(1-2):34-54.
- 28 86. Pedersen ME, Haegebaert RMS, Ostergaard J, Jensen H. Size-based
- 29 characterization of adalimumab and TNF-alpha interactions using flow induced
- 30 dispersion analysis: assessment of avidity-stabilized multiple bound species. *Sci Rep*.
- 31 2021;11(1):10.
- 32 87. Hong J, Wu HM, Zhang RK, He MY, Xu W. The Coupling of Taylor Dispersion
- 33 Analysis and Mass Spectrometry to Differentiate Protein Conformations. *Anal Chem*.
- 34 2020;92(7):5200-6.
- 35 88. Labied L, Rocchi P, Doussineau T, Randon J, Tillement O, Lux F, et al. Taylor
- 36 Dispersion Analysis Coupled to Inductively Coupled Plasma-Mass Spectrometry for
- 37 Ultrasmall Nanoparticle Size Measurement: From Drug Product to Biological Media
- 38 Studies. *Anal Chem*. 2021;93(3):1254-9.
- 39 89. Saetear P, Chamieh J, Kammer MN, Manuel TJ, Biron JP, Bornhop DJ, et al.
- 40 Taylor Dispersion Analysis of Polysaccharides Using Backscattering Interferometry.
- 41 *Anal Chem*. 2017;89(12):6710-8.
- 42 90. Pusey PN, Vanmegen W. DETECTION OF SMALL POLYDISPERSITIES BY
- 43 PHOTON-CORRELATION SPECTROSCOPY. *J Chem Phys*. 1984;80(8):3513-20.
- 44 91. Liu T, Oukacine F, Collet H, Commeyras A, Vial L, Cottet H. Monitoring surface
- 45 functionalization of dendrigraft poly-L-lysines via click chemistry by capillary
- 46 electrophoresis and Taylor dispersion analysis. *J Chromatogr A*. 2013;1273:111-6.
- 47 92. Deschamps J, Dutremez SG, Boury B, Cottet H. Size-Based Characterization of
- 48 an Ionic Polydiacetylene by Taylor Dispersion Analysis and Capillary Electrophoresis.
- 49 *Macromolecules*. 2009;42(7):2679-85.
- 50
- 51
- 52
- 53
- 54
- 55
- 56
- 57
- 58
- 59
- 60

- 1  
2  
3 93. Le Saux T, Cottet H. Size-based characterization by the coupling of capillary  
4 electrophoresis to Taylor dispersion analysis. *Anal Chem.* 2008;80(5):1829-32.  
5 94. Oukacine F, Geze A, Choisnard L, Putaux JL, Stahl JP, Peyrin E. Inline Coupling  
6 of Electrokinetic Preconcentration Method to Taylor Dispersion Analysis for Size-Based  
7 Characterization of Low-UV-Absorbing Nanoparticles. *Anal Chem.* 2018;90(4):2493-  
8 500.  
9 95. Leclercq L, Cottet H. Fast Characterization of Polyelectrolyte Complexes by  
10 Inline Coupling of Capillary Electrophoresis to Taylor Dispersion Analysis. *Anal Chem.*  
11 2012;84(3):1740-3.  
12 96. He MY, Luo P, Hong J, Wang XF, Wu HM, Zhang RK, et al. Structural Analysis  
13 of Biomolecules through a Combination of Mobility Capillary Electrophoresis and Mass  
14 Spectrometry. *ACS Omega.* 2019;4(1):2377-86.  
15 97. Zhang RK, Wu HM, He MY, Zhang WJ, Xu W. Mobility Capillary Electrophoresis-  
16 Restrained Modeling Method for Protein Structure Analysis in Mixtures. *J Phys Chem B.*  
17 2019;123(10):2335-41.  
18 98. Zhang WJ, Wu HM, Zhang RK, Fang X, Xu W. Structure and effective charge  
19 characterization of proteins by a mobility capillary electrophoresis based method. *Chem*  
20 *Sci.* 2019;10(33):7779-87.  
21 99. Wu HM, Zhang RK, Zhang WJ, Hong J, Xiang Y, Xu W. Rapid 3-dimensional  
22 shape determination of globular proteins by mobility capillary electrophoresis and native  
23 mass spectrometry. *Chem Sci.* 2020;11(18):4758-65.  
24 100. Beard DA, Wu F. Apparent Diffusivity and Taylor Dispersion of Water and  
25 Solutes in Capillary Beds. *Bulletin of Mathematical Biology.* 2009;71(6):1366-77.  
26 101. Callendar R, Leaist DG. Diffusion coefficients for binary, ternary, and  
27 polydisperse solutions from peak-width analysis of taylor dispersion profiles. *J Solut*  
28 *Chem.* 2006;35(3):353-79.  
29 102. Ghanavati M, Hassanzadeh H, Abedi J. Application of taylor dispersion technique  
30 to measure mutual diffusion coefficient in hexane plus bitumen system. *Aiche J.*  
31 2014;60(7):2670-82.  
32 103. Biron JP, Bonfils F, Cipelletti L, Cottet H. Size-characterization of natural and  
33 synthetic polyisoprenes by Taylor dispersion analysis. *Polymer Testing.* 2018;66:244-  
34 50.  
35 104. Jin XY, Leclercq L, Sisavath N, Cottet H. Investigating the Influence of  
36 Phosphate Ions on Poly(L-lysine) Conformations by Taylor Dispersion Analysis.  
37 *Macromolecules.* 2014;47(15):5320-7.  
38  
39  
40  
41  
42  
43  
44  
45  
46  
47  
48  
49  
50  
51  
52  
53  
54  
55  
56  
57  
58  
59  
60